Title: Emergence and fate of stem cell-like *Tcf7*$^+$ CD8$^+$ T cells during a primary immune response to viral infection

Authors: Joana Gomes Silva[1,†], Daniela Pais Ferreira[1,†,‡], Alexandre Dumez[1,†], Tania Wyss[2], Romain Veber[1], Maxime Danilo[1,§], Daniel D. Pinschewer[3], Mélanie Charmoy[1] and Werner Held[1,*]

Affiliations:

[1] Department of Oncology, University of Lausanne, Lausanne, Switzerland

[2] SIB Swiss Institute of Bioinformatics, Bioinformatics Core Facility, Lausanne, Switzerland.

[3] Department of Biomedicine, Division of Experimental Virology, University of Basel, Switzerland

*Corresponding author. Email: Werner.Held@unil.ch

† Equal contribution

Present address

‡ Ichnos Sciences Biotherapeutics SA, Epalinges, Switzerland

§ Department of Oncology, Centre Hospitalier Universitaire Vaudois, Lausanne, Switzerland

One Sentence Summary: Priming yields stem-like T cells that are prone to become central memory but can be deviated towards an effector fate by inflammation.

Abstract: In response to infection, naïve $CD8^+$ T cells (T_N) yield a large pool of short-lived terminal effector (T_{TE}) cells that eliminate infected host cells. In parallel, a minor population of stem cell-like central memory (T_{CM}) cells forms, that has the capacity to maintain immunity following pathogen clearance. It has remained uncertain whether stem-like T_{CM} cells arise by de-differentiation from a subset of cytolytic T_{TE} cells or whether priming generates stem-like cells capable of seeding the T_{CM} compartment and, if so, when cytolytic T_{TE} cells branch-off. Here, we show that $CD8^+$ T cells with stem-like properties, which are identified by the expression of TCF1 (encoded by *Tcf7*), are present across the primary response to infection. Priming programs T_N cells to undergo multiple cell divisions, over the course of which TCF1 expression is maintained. These $TCF1^+$ cells further expand relatively independently of systemic inflammation, antigen dose or affinity and they quantitatively yield $TCF1^+$ T_{CM} cells following pathogen clearance. Inflammatory signals suppress TCF1 expression in early divided $TCF1^+$ cells. TCF1 downregulation is associated with the irreversible loss of self-renewal capacity and the silencing of stem/memory genes, which precedes the stable acquisition of a T_{TE} state. TCF1 expression restrains cell cycling, explaining in part the limited expansion of $TCF1^+$ relative to $TCF1^-$ cells during the primary response. Thus, our data are consistent with terminal differentiation of effector cells being a step wise process that is initiated by inflammation in primed stem-like cells, that would otherwise become central memory cells by default.

Main Text:

INTRODUCTION

Infection activates very rare naïve antigen-specific $CD8^+$ T cells (T_N), which expand and differentiate into cytolytic effector cells that are needed to clear pathogen-infected cells. While most of the effector $CD8^+$ T cells are terminally differentiated and die following pathogen clearance (referred to as T_{TE} cells), 5–10% of the responding cells persist following pathogen clearance and form a diverse memory $CD8^+$ T cell compartment. The latter includes central memory T cells (T_{CM}) which maintain immunity to subsequent infections with the same pathogen thanks to their stem cell-like potential to expand, differentiate into effector cells or self-renew (*1*). Several models have been proposed to explain the relationship between the distinct $CD8^+$ T cell states, the predominance of effector cells during the acute phase of the immune response and the emergence of memory cells after antigen clearance (*2-5*). The linear differentiation model suggests that T_N cells expand and acquire cytotoxic capacity. Once infection is cleared, occasional cells de-differentiate to become non-cytolytic T_{CM} cells (*6, 7*). De-differentiation is not random, as one subpopulation of effector stage $CD8^+$ T cells, termed memory precursor effector cells (MPEC), are biased towards memory fate (*8-10*) although they do not quantitatively yield memory. Irrespectively, MPEC cells express Granzyme B and have cytotoxic activity (*8*) and would, thus, need to de-differentiate to yield non-cytolytic T_{CM} cells. In support of this model, the *Sell* locus (encoding CD62L) has inhibitory DNA methylation marks in MPEC, but is demethylated in T_{CM} cells (*7*). Alternative scenarios include the so-called progressive differentiation model, which proposes that short-lived effector cells derive from precursors of long-lived cells (*2-5, 11-14*). Indeed, epigenetic repression of memory associated genes is needed for efficient effector differentiation (*15-17*). Here, the level of antigenic, costimulatory and inflammatory signals that individual cells accumulate is thought to determine the proliferation and differentiation of these precursors. According to this model, stem-like cells would be required to be present throughout the primary response to infection, however, that had not been formally demonstrated.

The developmental relationship between T_{CM} and T_{TE} cells may be followed using the expression of the transcription factor TCF1 (encoded by the *Tcf7 gene*), which is required for the generation of T_{CM} cells but dispensable for T_{TE} formation (*18-20*). T_N cells express high levels of TCF1 and most $CD8^+$ T cells lose expression after day 3 of LCMV infection and this is associated with

effector differentiation. However, a small population of *Tcf7*$^+$ cells is detected throughout the primary response to infection (*21, 22*). In addition, effector stage cells expressing the central memory marker CD62L have been observed in bacterial (*Listeria monocytogenes; L.m.*) (*23-25*) and LCMV infection *(26)* where they overlap in part with *Tcf7*$^+$ cells (*22*). *Tcf7*$^+$ cells present during the expansion phase (day 5 post LCMV infection) have the potential to yield T_{CM} cells following transfer into infection-time matched secondary hosts. On the other hand d5 *Tcf7*$^-$ cells fail to yield T_{CM} cells and remain *Tcf7*$^-$ (*21*). Lineage tracing subsequently revealed that the *Tcf7*$^+$ cells present at the peak of the response (d8) quantitatively and exclusively yield T_{CM} cells (*22*) in line with the inferred trajectory of such cells based on scRNAseq analysis (*27*). The d8 *Tcf7*$^+$ cells, thus, qualify as central memory precursors (T_{pCM}). T_{pCM} cells closely resemble T_{CM} cells as judged by their comparable phenotype, lack of cytolytic activity and stem cell-like potential in recall stimulation experiments, whereby TCF1 is essential for the self-renewal of T_{pCM} cells (*22*). The presence of stem-like *Tcf7*$^+$ CD8$^+$ T cells at the peak of the response indicated that *Tcf7*$^+$ cells might display stem cell-like potential and central memory precursor function throughout the primary response to infection. If so, it was unknown when and under what conditions these *Tcf7*$^+$ cells committed towards differentiation, and how this translated into changes in stemness and effector programs.

Here, we show that TCF1$^+$ CD8$^+$ T cells maintain stem cell-like potential and central memory precursor function throughout the primary immune response, but that only the TCF1$^+$ cells present during priming can yield TCF1$^-$ T_{TE} cells. Priming programs cells to undergo multiple cell divisions while retaining TCF1. The presence of type I IFN during the cell division, rather than the priming phase, downregulates TCF1 resulting in the stable loss of stemness. Thus, dividing TCF1$^+$ cells that are committed to become T_{CM} cells, can be deviated towards T_{TE} differentiation by inflammatory cytokine-induced TCF1 suppression.

RESULTS

Tcf7^{+} CD8^{+} T cells are present throughout the primary immune response to infection

We have recently shown that *Tcf7*$^{+}$ CD8^{+} T cells present at the peak of the primary response to LCMV (Lymphocytic choriomeningitis virus) infection display key features of T_{CM} cells (*22*). Here, we used scRNAseq to address whether transcriptionally similar cells were present throughout the primary CD8^{+} T cell response to infection. We adoptively transferred naïve P14 CD8^{+} T cells (CD45.2), which express a transgenic T cell receptor (TCR) specific for the LCMV gp33-41 epitope presented by H-2D^{b}, into C57BL/6 (B6) recipients (CD45.1 or CD45.1/2). Mice were then infected with LCMV strains, which cause acute resolving infection. On d0 (naïve), d2, d3, d4 and d6 post-infection, splenic P14 cells were identified (**fig. S1, A and B**), flow sorted and subjected to scRNAseq analysis, obtaining 19,374 high-quality cells for further analysis (**Data file S1)**.

Compared to T_N cells (d0), the average number of unique molecular identifiers (UMIs) and genes was transiently increased in d2 and d3 cells (**fig. S1C**). Based on uniform manifold approximation and projection (UMAP) dimensionality reduction, T_N (d0), d2 and d6 cells were portioned into discrete areas, while d3 and d4 cells partially co-mingled, indicating substantial transcriptome changes (**Fig. 1A**). We addressed whether cells that were transcriptomically similar to T_{pCM} cells were present throughout the primary immune response. To this end, we calculated a T_{pCM} gene signature score (**Data file S2**) (*22*). While almost all T_N and d2 cells had a positive T_{pCM} score, the presence of such cells was reduced on d3, d4 and d6 post infection (p.i.). Notwithstanding, T_{pCM}, score-positive and *Tcf7*$^{+}$ cells were detected at each time point (**Fig. 1, B to D**). Very similar results were obtained using a T_{CM} gene signature score (**fig. S1D**) (**Data file S2**) (*22*).

To track and eventually isolate TCF1 expressing P14 cells during the primary immune response we used a *Tcf7*^{GFP} reporter mouse strain (*28*). *Tcf7*^{GFP} was highly expressed in virtually all T_N and most d2 cells, but was downregulated in most cells from d4 p.i. However, 2-10% of cells retained *Tcf7*^{GFP} expression in response to a low dose ($2x10^5$ plaque forming units (pfu)) of LCMV Armstrong (Arm) strain (**Fig. 1E**), a 10-fold higher LCMV Arm dose (**fig. S1, E and F**) or in response to LCMV WE (*22*), a LCMV strain with broader tissue tropism compared to Arm (*29*). The *Tcf7*$^{GFP+}$ cells expanded between d4 and d6 p.i. although at a reduced rate compared to *Tcf7*$^{GFP-}$

cells (**Fig. 1F**). A considerable fraction of the *Tcf7*$^{GFP+}$ cells expressed CD62L, CD127, IFNγ and IL-2 at all timepoints, while a subset of these cells expressed GzmB (but not GzmA) at d2 and d4 but not at later stages of the primary response (**fig. S2**) as shown before (*22*). Thus, CD8$^+$ T cells with phenotypic and transcriptional similarity to T_{pCM} and T_{CM} cells were present throughout the primary response to acute infection.

The stem-like potential of *Tcf7*$^+$ CD8$^+$ T cells is retained throughout the primary immune response

Tcf7 is expressed by CD8$^+$ T cells with stem-cell like potential. Therefore, we investigated whether the early *Tcf7*$^{GFP+}$ cells had the capacity to expand and self-renew or differentiate in response to recall stimulation. We isolated *Tcf7*$^{GFP+}$ and *Tcf7*$^{GFP–}$ P14 cells from the various time points of infection and re-transferred them into naïve secondary recipients that were then infected with LCMV. Eight days later (dx+8), *Tcf7*$^{GFP+}$ cells had expanded approximately 10^4-fold, irrespective of the time point of isolation from primary hosts, very similar to that of T_N (d0+8) or T_{CM} cells (d28+8) (**Fig. 1G**). *Tcf7*$^{GFP+}$ cells yielded more progeny than *Tcf7*$^{GFP-}$ cells isolated from the same time point (**Fig. 1G**). Primary *Tcf7*$^{GFP-}$ cells produced only *Tcf7*$^{GFP-}$ offspring, most of which had a T_{TE} phenotype (Klrg1$^+$ CD127$^-$ CD62L$^-$) (**Fig. 1H, fig. S3).** Primary *Tcf7*$^{GFP+}$ cells yielded more diverse progeny including *Tcf7*$^{GFP-}$ Klrg1$^+$, *Tcf7*$^{GFP-}$ Klrg1$^-$ as well as secondary *Tcf7*$^{GFP+}$ cells (**Fig. 1H, fig. S3**). The latter lacked Klrg1, but frequently expressed CD127 and occasionally CD62L (**fig. S3**). Secondary *Tcf7*$^{GFP+}$ cells derived comparably from T_N and d2 *Tcf7*$^{GFP+}$ cells, but were generated less efficiently from later *Tcf7*$^{GFP+}$ cells, although the output was still equivalent or superior in number to that from T_{CM} cells (d28+8) (**Fig. 1H**). The regeneration capacity of *Tcf7*$^{GFP+}$ cells thus declined with the progression of the primary response (**Fig. 1H**). This decline was not related to a change in the fraction of *Tcf7*$^+$ cells co-expressing CD62L (**fig. S2A**). Moreover, the d8 *Tcf7*$^+$ CD62L$^+$ and *Tcf7*$^+$ CD62L$^-$ subsets had comparable recall expansion and regeneration capacity, as judged by the generation of secondary *Tcf7*$^{GFP+}$ cells (**fig. S4)**. Thus, the presence of *Tcf7*$^+$ cells lacking CD62L at d8 p.i. did not explain the reduced stemness compared to d0 cells. We conclude that *Tcf7*$^+$ CD8$^+$ T cells retain stem-like potential throughout the immune response,

but that their regeneration capacity declines. The latter may be related to the number of prior cell divisions, as recently suggested for T_{CM} cells (*30*).

$Tcf7^+$ $CD8^+$ T cells maintain the capacity to become T_{CM}, but their ability to form differentiated subsets declines with time after infection

Since $Tcf7^+$ $CD8^+$ T cells had stem cell-like potential as judged by the response to recall stimulation, we next addressed their capacity to yield short-lived effector cells (T_{TE}) or memory cell subsets (T_{CM}, effector memory (T_{EM}) or tissue resident memory (T_{RM})) during the immune response. We used a *Tcf7*-guided fate mapping approach, based on a $Tcf7^{GFP\text{-}CreERT2}$ mouse strain ($Tcf7^{GFP\text{-}iCre}$) (*22*) combined with a $Rosa26^{TdTomato}$ ($R26^{Tom}$) reporter allele, to determine the fate of the stem-like $CD8^+$ T cells during a primary immune response without adoptive cell transfers. A single dose of Tamoxifen (TAM) induced Tom expression in a sizeable fraction of $Tcf7^+$ cells whereby the effective TAM half-life was around 12h (**fig. S5**).

In our previous work, when fate mapping was initiated on d8 post LCMV infection, we found that virus-specific d8 $Tcf7^+$ cells yielded $Tcf7^+$ T_{CM} but essentially no $Tcf7^-$ T_{EM} or short-lived T_{TE} cells (*22*). To determine whether $Tcf7^+$ $CD8^+$ T cells yielded T_{CM} or differentiated $Tcf7^-$ progeny at earlier time points of infection, we initiated fate-mapping on d1, d2, d3 or d4 p.i. (**Fig. 2A**). Tom-labelled $CD8^+$ T cells, that retained $Tcf7^{GFP}$ expression (Tom^+ $Tcf7^{GFP\text{-}iCre+}$), were observed both on d8 and d28 p.i., irrespective of when labeling was started (**Fig. 2, B and E)**. Some of these Tom^+ $Tcf7^{GFP\text{-}iCre+}$ cells expressed CD62L and most lacked Klrg1 both at d8 and d28 p.i. (**Fig. 2, C and F**), consistent with a T_{pCM}/T_{CM} phenotype. The abundance of Tom^+ $Tcf7^{GFP\text{-}iCre+}$ cells at d8 and at d28 p.i. was comparable (**Fig. 2H**), indicating that $Tcf7^+$ $CD8^+$ T cells quantitatively generated T_{CM} cells. Similar data were obtained when fate mapping was performed using a $Rosa26^{lox\ stop\ lox\ Confetti}$ ($R26^{Confetti}$) reporter allele (**fig. S6**). Fate mapping, thus, showed that $Tcf7^+$ cells present throughout the primary response gave rise to T_{CM} cells and thus qualified as T_{pCM} cells.

In addition, fate-mapping of $Tcf7^+$ cells at d1, d2, d3 or d4 yielded Tom^+ memory cells (d28 p.i.) that no longer expressed *Tcf7* (Tom^+ $Tcf7^{GFP\text{-}iCre\text{-}}$) (**Fig. 2, E and I**). These cells lacked CD62L but many expressed Klrg1 (**Fig. 2G**), consistent with a T_{EM} phenotype. The ability of $Tcf7^+$ cells to

yield *Tcf7*$^{-}$ memory cells declined as the primary response progressed (**Fig. 2I**), and we have previously shown this no longer occurred from d8 T*cf7*$^{+}$ cells (*22*). Tom^{+} *Tcf7*$^{GFP\text{-}iCre\text{-}}$ cells were also observed at the peak of the primary response (d8 p.i.) (**Fig. 2, B and J**). These cells lacked CD62L but most of them expressed Klrg1 (**Fig. 2D**).

When labeling of *Tcf7*$^{+}$ cells was started at d1 or d2, Tom^{+} *Tcf7*$^{GFP\text{-}iCre\text{-}}$ cells were more abundant at d8 than at d28 (**Fig. 2J**), consistent with d1,2 *Tcf7*$^{+}$ cells generating short-lived T_{TE} cells that disappeared following viral clearance. In contrast, the abundance of Tom^{+} *Tcf7*$^{GFP\text{-}iCre\text{-}}$ cells at d8 and d28 was not different when labelling was started at d3 or d4 (**Fig. 2J**), indicating that T_{TE} cells were no longer generated. Corresponding data were obtained when lineage tracing was performed using a *R26*^{Confetti} reporter allele (**fig. S6**). Moreover, fate mapping of antigen-specific *Tcf7*$^{+}$ cells, recognizing the gp33 and the np396 epitopes, from a polyclonal population confirmed that d4 *Tcf7*$^{+}$ cells yielded *Tcf7*$^{+}$ and *Tcf7*$^{-}$ memory cells but not short-lived T_{TE} cells (**fig. S7, A to F**). Additionally, d2 *Tcf7*$^{+}$ cells were the main source of T_{RM} cells present among intestinal intraepithelial lymphocytes (IEL) at d28 p.i. (**fig. S7, G to I**).

To confirm that *Tcf7*$^{+}$ cells did not yield T_{TE} cells after d2 p.i., we delayed the adoptive transfer of naïve P14 cells relative to the time of infection (**Fig. 3A**). Compared to the transfer of naïve P14 cells at the time of infection (d0), P14 transfer at d3 p.i. resulted in a 41.9-fold reduced expansion of P14 cells at d8 p.i. (**Fig. 3B**). Interestingly, the formation of *Tcf7*$^{GFP\text{-}}$ Klrg1^{+} P14 cells was reduced 107-fold, while that of *Tcf7*$^{GFP+}$ P14 cells was only reduced 5.5-fold (**Fig. 3C**). The latter cells expressed CD62L and produced IL-2 (**fig. S8**), similar to T_{pCM} cells.

Thus, our data are consistent with *Tcf7*$^{+}$ cells having stemness, and maintain the ability to form T_{CM} cells, but that they are unable to become T_{TE} and T_{RM} cells efficiently after d2 and cease to yield T_{EM} cells between d4 and d8 p.i.. Moreover, our data indicate that the antigenic/inflammatory environment at d3 p.i. generated *Tcf7*$^{+}$ cells relatively efficiently but did no longer result in T_{TE} formation.

$Tcf7^+$ $CD8^+$ T cells no longer contribute to the pool of short-lived effectors 4 days post infection but seed memory subsets

Despite the presence of $Tcf7^+$ $CD8^+$ T cells throughout the immune response, fate mapping suggested that these cells no longer contributed to the T_{TE} pool after d4 p.i.. To independently address this, we utilized T cells from $Tcf7^{DTR\text{-}GFP}$ transgenic mice (*31*), whereby the expression of the diphtheria toxin receptor (DTR) allowed *Tcf7*-expressing cells to be selectively ablated *in vivo*. We transferred $Tcf7^{DTR\text{-}GFP}$ (or control $Tcf7^{GFP}$) P14 cells to B6 mice, and treated with Diphtheria Toxin (DT) at d4 and d5 post LCMV Arm infection (**Fig. 3D**). At d6 p.i. the spleen of mice transferred with $Tcf7^{DTR\text{-}GFP}$ P14 cells harbored 48-fold fewer $Tcf7^+$ P14 cells than control mice, while the number of $Tcf7^-$ P14 cells was not different (around 10^6 cells) (**Fig. 3E**) demonstrating that DT treatment ablated selectively $Tcf7^+$ cells. Independent of the ablation of $Tcf7^+$ P14 cells, $Tcf7^-$ P14 cells had expanded to around 10^7 cells at d8 (**Fig. 3 F)** and both had contracted at d16 p.i., (**Fig. 3, F and G**), indicating that the short-lived effector T_{TE} cell pool indeed derived from $Tcf7^-$ rather than $Tcf7^+$ cells present on d4 of the infection.

We evaluated the memory compartment at 16 p.i., as the mice lose weight around 10 days following DT injection (d14 p.i.) independently of the presence of DT-sensitive cells (*32*). We found that the deletion of d4 $Tcf7^+$ cells reduced presence of $Tcf7^-$ cells (T_{EM}) (4.6-fold) (**Fig. 3G**) and that of $CD62L^+$ $Klrg1^-$ (52-fold) and $IL\text{-}2^+$ cells (6-fold) (T_{CM}) (**Fig. 3, H and I**), indicating that the formation of T_{EM} and T_{CM} did depend on d4 $Tcf7^+$ cells. In contrast, as previously found, d10 $Tcf7^+$ cells do not yield T_{EM} but are essential to form a T_{CM} compartment (*22*) confirming that that the capability of $Tcf7^+$ cells to yield T_{EM} cells ceases over time.

Finally, we analyzed the data for evidence that $Tcf7^-$ cells re-acquired *Tcf7* expression during the expansion or the maintenance phase. Control $Tcf7^{GFP+}$ cells expanded 7.6-fold from d6 to d8 p.i., very similar to that of residual *Tcf7*-expressing $Tcf7^{DTR\text{-}GFP}$ cells in DT-treated mice. Moreover, the abundance of these $Tcf7^+$ cells did not change between d8 and d16 p.i. (**Fig. 3J**). There was thus no evidence that $Tcf7^-$ cells re-acquired *Tcf7* expression, indicating that the *Tcf7* locus in d4 $Tcf7^-$ cells was stably silenced.

Low TCR and inflammatory signaling favor T_{pCM} relative to T_{TE} formation

Our data suggested that signals early in the immune response determined whether $CD8^+$ T cells maintained or downregulated the expression of *Tcf7*. To identify signals that could be responsible for modulating early responding $CD8^+$ T cells, we used our scRNA-seq data to evaluate the enrichment of Pathway Interaction Database (PID) (*33*) and Hallmark (*34*) pathway genes in *Tcf7*$^+$ or *Tcf7*$^-$ cells. Compared to T_N cells, $CD8^+$ T cells from d2 p.i., that were essentially all *Tcf7*$^+$, were enriched for the IFNα, IL-12 (PID) and CD8_TCR downstream pathways (**Fig. 4A**) However, genes associated with the the TCR_pathway (PID), which includes components of the TCR complex (*CD3e, CD3g, Lck*), were downregulated (**Fig. 4A**), consistent with cells undergoing TCR stimulation (*35*). Downregulation of the TCR_pathway was less profound in d3 cells and no longer observed in d4 *Tcf7*$^+$ cells. In comparison, the downregulation of the TCR_pathway was stronger and more sustained in *Tcf7*$^-$ cells (**Fig. 4A**) compared to T_N cells. Thus, these data suggest that *Tcf7*$^+$ $CD8^+$ T cells are transiently exposed to TCR and inflammatory signals.

The quantity and the quality of TCR signals determines the expansion of antigen-specific cells (*36, 37*). To address the role of antigen dose and TCR affinity in T_{pCM} formation we used LCMV cl13 virus strains harboring altered gp33 epitopes. While the P14 TCR has no measurable affinity for the F38L (KAVYN**L**ATC) (Δgp33) epitope (*38*), the affinity for the A39C epitope is around 100-fold reduced compared to the wild-type epitope (*39*). WT mice harboring P14 cells were infected with mixtures of WT and F38L (Δgp33) LCMV cl13 that ranged from 100%, 30%, 10%, 3% to 0% of WT virus (**Fig. 4B**). The total infectious dose was kept low (200 pfu) to obtain resolved infection and constant to provide comparable infectious and inflammatory environments. Indeed, the mixtures induced very similar endogenous $CD8^+$ T cell responses to the np396 epitope (**fig. S9A**). As expected, P14 cells did not respond to infection with the F38L virus. Progressively increasing the contribution of WT virus to the mixture resulted in a proportional increase in the abundance of P14 cells at d8 p.i. (**Fig. 4C**). At the lowest antigen dose (3%), the fraction of *Tcf7*$^+$ cells among the total pool of P14 cells was increased (**Fig. 4D**) and consequently that of *Tcf7*$^-$ cells was decreased. Despite minor differences, the responding P14 subsets had comparable phenotypes (**fig. S9, B and C**), indicating that T_{pCM} formation was less sensitive to a low antigen dose compared to T_{TE} formation. Infection with the LCMV variant expressing the low affinity A39C

epitope resulted in a 14.5-fold reduced expansion of P14 cells (**Fig. 4E**) that harbored an increased fraction of *Tcf7*$^{GFP+}$ cells compared to the infection with WT LCMV (**Fig. 4F**). Despite some differences, the responding P14 subsets had a comparable phenotype (**Fig. 4, G and H**). In addition, the different virus variants induced a similar response by endogenous np396-specific CD8$^+$ T cells (**fig. S9D**). Thus, the formation of T_{pCM} cells was less affected by low antigen dose and affinity than the generation of T_{TE} cells.

We then investigated how T_{pCM} formation was influenced by inflammatory signals. Exposure to IL-2, IL-12 and type-I interferon (IFN-I) provides survival factors and promotes effector differentiation (*8, 14, 40*). Since IFN-I, rather than IL-12, is essential for effector differentiation in response to LCMV infection (*41, 42*), we addressed the importance of IFNAR signaling in T_{pCM} formation. IFNAR blockade resulted in 15.2-fold reduction of P14 cells, whereby *Tcf7*$^{GFP-}$ and *Tcf7*$^{GFP-}$ Klrg1$^+$ T_{TE} cells were reduced 23.7-fold and 293-fold, respectively. In contrast, the abundance of *Tcf7*$^{GFP+}$ cells was unaltered (**Fig. 5, A and B**). Although these cells showed normal CD62L expression, IL-2 production was reduced (**Fig. 5, C and D)**. In addition, PD-1 and Lag3 expression was increased compared to controls (**fig. S9E**). The latter may be related to the fact that IFNAR blockade augments LCMV loads and delays viral clearance (*43*). However, the protracted infection does not account for the lack of Klrg1$^+$ cells, as such cells are readily observed at d8 post LCMV cl13 infection (*44*). These data showed that IFN-I signaling was essential for T_{TE} but dispensable for T_{pCM} formation.

T_{pCM} cells are generated in response to dendritic cell vaccination

As a complementary approach to address the role of inflammatory signals in the formation of T_{pCM}, we investigated their generation in response to dendritic cell (DC) vaccination. Mice adoptively transferred with *Tcf7*^{GFP} P14 cells were vaccinated with LPS-matured and gp33 peptide-pulsed DC (termed DC33) alone or in combination with systemic exposure to the TLR9 ligand CpG-B (DC33+CpG) to induce systemic inflammation (*13, 45*). DC33 and DC33+CpG vaccination induced a comparable expansion of P14 cells at d7 post vaccination (**Fig. 5E**) consistent with previous work (*20*) (*45*). In response to DC33+CpG vaccination, most P14 cells had a *Tcf7*$^{GFP-}$ Klrg1$^+$ phenotype but 10% were *Tcf7*$^{GFP+}$ (**Fig. 5, F and G**). In comparison, DC33 vaccination generated fewer Klrg1$^+$ *Tcf7*$^{GFP-}$ and more *Tcf7*$^{GFP+}$ cells (**Fig. 5, F and G**). There was a similar

frequency of CD62L-expressing cells within the *Tcf7*$^{GFP+}$ CD8+ T cell population in both vaccination conditions, however the frequency of IL-2-producing cells was reduced following DC33+CpG vaccination (**Fig. 5, G and H**). Thus, absence of systemic inflammation resulted in an increased generation of cells with a T_{pCM} phenotype in response to DC vaccination.

DC33 vaccination expanded T_{pCM} cells around 200-fold relative to the input of naïve P14 cells (**Fig. 5F**), which was very similar to the response to LCMV infection (**Fig. 1F**). In comparison, vaccination with gp33 peptide or gp33 peptide plus adjuvant (poly(I:C) (pIC)) did not expand *Tcf7*$^{GFP+}$ P14 cells (showing signs of antigen-exposure (CD44^{+})) relative to input (**fig. S9F**). Although the requirements to generate T_{pCM} cells appeared less stringent than for T_{TE} cells, certain vaccination approaches failed to efficiently yield T_{pCM} cells.

Inflammatory signals received after priming, and once cells have committed to cell division, contribute to TCF1 downregulation in CD8^{+} T cells

We next investigated the relative importance of priming versus inflammatory cues during the early immune response to commit cells to divide and downregulate TCF1. CTV-labelled P14 cells were undivided and TCF1 protein was expressed at high levels 2 days after infection, but cell division and downregulation of TCF1 had occurred by d3.5 p.i. (**Fig. 6B, fig. S10A**). At this timepoint we observed non-divided TCF1^{+}, TCF1^{+} cells that had undergone 1-3 and >3 divisions as well as TCF1^{-} cells that had divided >3 times (**Fig. 6B**), in agreement with previous work (*21*).

To address the importance of inflammation in TCF1 downregulation and cell division, we treated mice with anti-IFNAR prior to adoptive cell transfer and infection. When IFNAR was blocked, all cells were divided **(Fig. 6B)**, which is likely explained by augmented viral antigen exposure (*46*). In addition, IFNAR blockade increased the fraction of highly divided (>3 divisions) TCF1^{+} relative to TCF1^{-} cells **(Fig. 6B**) suggesting that IFN-I promoted the downregulation of TCF1 in dividing cells. Cell division has been shown to be necessary for TCF1 downregulation based on *in vitro* experiments (*20, 21*).

We next addressed whether TCF1 expression and cell division was impacted by IFN-I exposure during the priming and/or the cell division phase. P14 cells were primed *in vivo,* and flow sorted on d2 p.i. when cells were undivided and expressed high levels of TCF1. Sorted cells were then cultured *in vitro* in the absence of additional signals except for the addition of naïve spleen cells and low dose IL-2 to ensure survival (**Fig. 6C**). After 48-72h of culture, P14 cells had undergone 0 to >4 cell divisions whereby all cells retained high TCF1 levels (**Fig. 6D**). TCF1 expression also remained high in cells primed *in vivo* in the presence of anti-IFNAR, despite the fact that most P14 cells were divided (**Fig. 6, D and F**). Thus, priming committed cells to divide multiple times but did not program TCF1 downregulation. Yet, addition of IFNβ during *in vitro* culture induced TCF1 downregulation in dividing cells (**Fig. 6, E and F**). This was also observed when cells had been primed in the absence of IFNAR signaling (**Fig. 6, E and F**). Similarly, when naïve P14 cells were activated with gp33 peptide-pulsed splenocytes *in vitro,* the presence of IL-12 during the division rather than the priming phase downregulated TCF1 (**fig. S10C**). Thus, the exposure of primed cells to inflammatory cytokines during the cell division phase was sufficient to induce TCF1 downregulation.

The absence of TCF1 increases the cycling of CD8$^+$ T cells

There is a disparity between the relatively high number of T_{TE} and smaller numbers of T_{pCM} generated during a primary immune response, which has been previously linked to relative rates of cell proliferation (*25*). Consistent with previous work, we observed that T_{CM}-prone TCF1$^+$ cells underwent fewer divisions than effector-prone TCF1$^-$ cells (**Fig. 6B, left**) (*21*). This raised the possibility that TCF1 protein itself limited the division of T_{CM}-prone cells. To address this issue, we crossed *Tcf7*^{GFP} reporter transgenic P14 mice to a *Tcf7*$^{-/-}$ background. Naïve P14 cells from these so-called KO *Tcf7*^{GFP} mice expressed the *Tcf7*^{GFP} reporter at high levels (*22*), and were thus useful to track *Tcf7*$^+$ (T_{pCM}) cells lacking TCF1 protein. At d3.5 p.i., WT and KO *Tcf7*^{GFP} cells had expanded comparably (**Fig. 6, G and H**) and subsets of both types of P14 cells retained *Tcf7*^{GFP} expression (**Fig. 6I**). While few WT *Tcf7*$^{GFP+}$ cells had divided >3 times, most KO *Tcf7*$^{GFP+}$ cells had divided >3 times (**Fig. 6J**). In contrast, all WT and KO *Tcf7*$^{GFP-}$ cells had divided >3 times (**Fig. 6J**).

We further evaluated the division of KO *Tcf7*^{GFP} cells at d4 and at d6 p.i using EdU incorporation during a 2h pulse. WT and KO *Tcf7*$^{GFP-}$ cells showed comparable frequencies of EdU$^+$ cells, which were increased compared to *Tcf7*$^{GFP+}$ cells (**fig. S10D**). Importantly, there were more KO *Tcf7*$^{GFP+}$ cells incorporating EdU than WT *Tcf7*$^{GFP+}$ cells (**fig. S10D**). Thus, *Tcf7*$^+$ cells lacking TCF1 protein underwent more cell divisions, suggesting that the accelerated cycling of *Tcf7*$^-$ cells is directly coupled to the downregulation of TCF1. These data are consistent with a role of TCF1 protein in limiting cell cycle entry or progression, providing an explanation for the preferential expansion of the *Tcf7*$^-$ T_{TE} compartment in response to infection.

Stable loss of the T_{pCM} gene signature occurs upon *Tcf7* downregulation and precedes stable acquisition of a T_{TE} gene signature

To obtain further insights into how the generation of T_{TE} cells from *Tcf7*$^+$ cells was controlled we computed a T_{TE} gene signature score derived from published data of d7 Klrg1$^+$ versus d7 Klrg1$^-$ cells (*47*) that was characterized by high expression of the genes of interest *Zeb2, CX3CR1, Klrg1* and *S1pr5* (**Fig. 7, A and B**) (**Data file S2**). We compared the distribution of T_{TE} versus the previously calculated T_{pCM} signature scores (**Data file S2**) in single CD8$^+$ T cells. The vast majority of d2 cells had a positive T_{pCM} but a negative T_{TE} score (**Fig. 7C**). Similarly, the vast majority of T_{pCM} score-positive cells at subsequent time points had a negative T_{TE} score (**Fig. 7C),** indicating that the two signatures rarely co-existed in single cells. Rather, some d2 cells, and the majority of the later cells, had a negative T_{pCM} score. These T_{pCM} negative cells lacked a T_{TE} signature at d2, while some d3 and most d4 cells had a weak T_{TE} score. Cells with a high T_{TE} score were first observed on d6 (**Fig. 7C**). Similar data were obtained using T_{CM} versus T_{EM}-derived signature scores (**Data file S2**) (**fig. S11, A and B**). Thus, these data suggested that CD8$^+$ T cells first downregulated the expression of T_{pCM} signature genes before upregulating T_{TE} signature genes.

We further addressed whether the transcriptional changes were related to changes in chromatin accessibility. To this end we performed ATACseq analysis of *Tcf7*$^+$(T_{pCM}), *Tcf7*$^-$ Klrg1$^-$ and *Tcf7*$^-$ Klrg1$^+$ (T_{TE}) cells isolated at d4 and d8 p.i. together with T_N cells and d28 *Tcf7*$^+$ (T_{CM}) and d28 *Tcf7*$^-$ cells (T_{EM}). While the different samples had comparable numbers of accessible regions, the sequencing coverage was lower in d4 *Tcf7*$^-$ cells (**fig. S11C**). This may be due to the rapid cycling

of most d4 cells (**fig. S10D**), which reduces chromatin accessibility (*48*). To address accessibility changes in T_{pCM} and T_{TE} signature genes, we integrated our bulk ATACseq data with previously-published bulk RNAseq data (*22*). Among the T_{pCM} genes overexpressed at the mRNA level (n=602), n=323 genes were more accessible in T_{pCM} cells, including the genes of interest *Tcf7, Sell and Ccr7* (**Fig. 7, D and F, fig. S11D)** (**Data file S3**). These genes contained a total of n=872 regions that were on average more accessible in T_{pCM} cells (**Fig. 7E**). These epigenetically regulated T_{pCM} genes and regions were also accessible in T_N, in d4 *Tcf7*$^{GFP+}$ as well as in d28 *Tcf7*$^{+}$ cells (T_{CM}). On the other hand, these genes/regions were less accessible in all *Tcf7*$^{GFP-}$ populations (**Fig. 7, D to F**). Motif search analysis showed that these less accessible regions were highly enriched for *Tcf7* binding motifs (**Fig. 7G)**. Thus, a considerable fraction of T_{pCM} genes contained *Tcf7* binding motifs and became less accessible and less expressed at the time point when *Tcf7* was downregulated, and this was associated with the loss of stemness.

Conversely, among genes overexpressed in T_{TE} cells (n=119), n=56 genes were more accessible in T_{TE} cells, including the genes of interest *Gzmb, Klrg1* and *Fasl* (**Fig. 7, D and I, fig S10E)** (**Data file S3**). These genes contained a total of n=152 regions that were more accessible in T_{TE} cells (d8 *Tcf7*$^{-}$ Klrg1^{+}) (**Fig. 7H**). The epigenetically regulated T_{TE} genes/regions were poorly accessible in all *Tcf7*$^{+}$ populations (T_N, d4, d8 and d28). T_{TE} genes/regions were also poorly accessible in d4 *Tcf7*$^{GFP-}$ Klrg1^{-} cells but gained some accessibility in the occasional d4 *Tcf7*$^{GFP-}$ Klrg1^{+} (**fig. S1F**) and in d8 *Tcf7*$^{GFP-}$ Klrg1^{-} cells, but reached maximal accessibility only in d8 *Tcf7*$^{GFP-}$ Klrg1^{+} (T_{TE}) cells (**Fig. 7, D, H and I, fig. S10E)**. Interestingly, the accessibility of T_{TE} genes in d28 *Tcf7*$^{-}$ (T_{EM}) cells was intermediate and corresponded to that seen in the d8 *Tcf7*$^{GFP-}$ Klrg1^{-} population **(Fig. 7H).** Many of these latter cells correspond to CD127^{+} Klrg1^{-} cells i.e. MPEC from which *Tcf7*$^{+}$ cells had been excluded (**fig. S2B**), suggesting that T_{EM} cells mainly derive from d8 *Tcf7*$^{-}$ CD127^{+} Klrg1^{-} cells. Even though T_{TE} genes were expressed in d4 *Tcf7*$^{-}$ cells, these genes became fully accessible only in *Tcf7*$^{-}$ Klrg1^{+} cells at d8 p.i. On the other hand, the *Ifng* locus was comparably accessible in *Tcf7*$^{+}$ and *Tcf7*$^{-}$ cells of the same time point, but was poorly accessible in T_N cells (**fig. S10F**), in agreement with IFNγ production (**fig. S2C**). The *Ifng* locus, thus, seemed to become accessible in response to activation and independent of T_{pCM}/T_{TE} differentiation. We concluded that the stable loss of stemness as seen in d4 *Tcf7*$^{-}$ cells preceded the stable acquisition of a T_{TE} program during CD8^{+} T cell differentiation.

DISCUSSION

The stage of an acute immune response when T cells commit to long-lived T_{CM} cells or to terminally differentiated effector cells has remained controversial. Here, we showed that a small population of $TCF1^+$ $CD8^+$ T cells with stem cell-like potential and T_{CM} precursor function was present throughout the primary response to infection. These $TCF1^+$ cells derived directly from primed naïve T cells whereby their expansion was proportional to the TCR signaling strength but independent of IFNAR signaling during infection or independent of systemic inflammation during DC vaccination. These findings are in line with earlier work showing that a brief stimulation of naïve $CD8^+$ T cells with antigen plus co-stimulation is sufficient for T_{CM} formation (*49, 50*) and DC vaccination in the absence of systemic inflammation results in accelerated T_{CM} formation (*13*). Thus, the default fate in response to T cell activation is the generation of $TCF1^+$ cells, which act as precursors of T_{CM} cells (T_{pCM}).

Prior work showed that T_{CM} cells preferentially derive from MPEC ($CD127^+$ $Klrg1^-$ effector cells), which have cytolytic activity (*8, 51*). To generate non-lytic T_{CM} cells, some MPEC would have to de-differentiate i.e. lose lytic activity and acquire stem-like properties following pathogen clearance (*6-8, 12, 51*). This linear differentiation scheme is supported by epigenetic changes of the *Sell* locus (encoding CD62L), which is demethylated in T_N cells, but has inhibitory DNA methylation marks in MPEC (and in short-lived effector cells ($CD127^-$ $Klrg1^+$)) and is again demethylated in T_{CM} cells (*7*). Similarly, the *Gzmb* locus is poorly accessible in T_N cells but is comparably accessible in MPEC and SLEC as well as in unfractionated memory cells (*52-54*). This suggested that all cells acquire an ‘‘effector-like’’ epigenetic program, and that dedifferentiation of some MPEC cells was needed for T_{CM} formation.

We recently reported that T_{CM} cells derive from d8 *Tcf7*$^+$ $CD8^+$ T cells, which represent a subset of around 10% of MPEC. These *Tcf7*$^+$ cells lack lytic activity and already have stem cell-like properties (*22*). However, as pathogen control is essentially complete at the peak of the primary response, it was possible that the d8 *Tcf7*$^+$ cells exist in the absence of antigen and that de-differentiation has already occurred. Here we showed that *Tcf7*$^+$ cells displaying T_{pCM} function and stem-like properties are present throughout the primary response to infection. Stemness was, thus, maintained in a subset of $CD8^+$ T cells in the presence of antigen rather than acquired subsequent

to pathogen clearance. The apparent inconsistency to prior data very likely derives from the fact that only 10% of MPEC are *Tcf7*$^+$ cells. Indeed, in contrast to MPEC, naïve/central memory genes (*Tcf7, Sell* or *Ccr7*) were accessible in T_{pCM} cells (d4 or d8 *Tcf7*$^+$), similar to T_N cells. Conversely, effector genes (*GzmB, Klrg1* or *FasL*) were poorly accessible in T_{pCM} and T_{CM} cells, and only modestly increased compared to T_N cells. These analyses thus suggested that T_{CM} cells derived from precursor cells that maintained stemness and that had not previously acquired a stable effector program. However, earlier work suggested that T_{CM} cells had expressed *GzmB* at some earlier stage (*6*). Some *Tcf7*$^+$ cells indeed expressed GzmB both at the mRNA and protein level until d4 of infection (**fig. S2D**) (*55*). Despite that, the accessibility of *GzmB* gene body (±5kb) in T_{pCM} cells (d4 or d8 *Tcf7*$^+$) was only slightly increased compared to T_N cells. Notwithstanding, an element 22kb upstream of the *GzmB* locus showed considerably increased accessibility in T_{pCM} and T_{CM} cells compared to T_N cells, providing evidence that the *GzmB* locus has been active in T_{CM} prone cells. Importantly, these cells did not acquire the chromatin accessibility changes associated with T_{TE} differentiation. The data, thus, suggest that T_{CM} cells derive from *Tcf7*$^+$ precursors without the need for de-differentiation.

The continuous presence of stem-like cells satisfied a key prediction of the progressive differentiation model. However, the stage during the immune response when stem-like cells committed to a T_{TE} fate remained unclear. Lineage tracing showed that only the TCF1$^+$ cells present during priming (i.e. prior to or around the first cell division) were competent to yield TCF1$^-$ T_{TE} cells, despite the fact that stem-like TCF1$^+$ cells were present throughout the primary immune response. Culturing *in vivo* primed, but undivided TCF1$^+$ cells showed that these cells were programmed to undergo several divisions, as shown before (*56*), whereby TCF1 expression was maintained. Addition of IFNβ during the division phase *in vitro* induced TCF1 downregulation, but prior IFNAR signaling *in vivo* was not needed. Thus, priming produced divided TCF1$^+$ cells that were committed to become T_{CM} cells and that could be diverted towards an effector fate by inflammatory cytokines, which suppressed TCF1. Prior work suggested that the effector versus memory fate decision is made based on a first asymmetric cell division, whereby the DC proximal daughter cell is effector-prone and the distal daughter cells is memory-prone (*9*). While there was no evidence of asymmetric TCF1 distribution during the first 3 cell divisions, see also (*21*), it remains possible that the initial cell division generates effector prone cells. However, such cells

may realize their potential only several generations later dependent on their exposure to inflammatory signals. Thus, priming generates T_{CM}-prone $TCF1^+$ cells and inflammation-dependent TCF1 downregulation initiates the diversion of some of these cells towards an effector fate.

Finally, we addressed the hierarchy of transcriptional and chromatin accessibility changes associated with differentiation. Previous data suggested that naïve cells, which express a stem/memory signature but lack an effector gene signature, give rise to cycling cells expressing both signatures. Such bipotent differentiation intermediates then commit towards effector cells by silencing the stem/memory signature (*17*). However, this hierarchy was deduced from a relatively late stage of the response to bacterial infection (day 7), while we obtained evidence for a stable cell fate change on d3.5-4 of the response, which occurred upon TCF1 downregulation. Indeed, TCF1 loss resulted in a reduced accessibility of the *Tcf7* locus and a subset of T_{pCM} signature genes. TCF1 downregulation was associated with the loss of T_{pCM} function and stemness and was stable, as there was no evidence that *Tcf7* was re-expressed by *Tcf7*$^-$ cells. Importantly, these early *Tcf7*$^-$ cells had not yet acquired a stable T_{TE} program. Thus, we propose that T_{TE} differentiation involves the stable loss of stemness, which occurs in response to inflammation-induced TCF1 downregulation and that this is followed by the stable acquisition of a T_{TE} state.

The current study has some limitations. The early phase of the response was studied using unphysiologically large numbers of virus-specific $CD8^+$ T cells, which reduces cellular activation and could thus explain the presence of $TCF1^+$ $CD8^+$ T cells early during the primary response. However, lineage tracing and lineage deletion experiments are based on lower numbers of input cells and the findings provide clear, although circumstantial evidence that $TCF1^+$ $CD8^+$ T cells were present throughout the primary response. Finally, the study does not address the question, how some primed cells retain TCF1 in the face of systemic inflammation.

A key goal of understanding the developmental origin of T_{CM} cells is to generate such cells by vaccination. The identification of T_{CM} precursor cells represents an important step towards that goal. Here we showed that DC vaccination (in the absence of systemic inflammation) leads to a 200-fold expansion of antigen-specific *Tcf7*$^+$ cells (compared to the input of naïve T cells), which

was remarkably similar to LCMV infection. Conversely, peptide plus adjuvant vaccination failed to amplify *Tcf7*$^{+}$ cells. These initial experiments highlight that *Tcf7*$^{+}$ cells can be expanded by vaccination but that the precise conditions will need to be defined and improved. The identification of TCF1^{+} T_{pCM} cells should greatly facilitate the optimization of current as well as the testing of approaches of candidate T cell vaccines.

MATERIALS AND METHODS

Study Design

The goal of this study was to understand the developmental origin of effector and memory CD8^{+} T cells in response to viral infection. TCR transgenic T cells, expressing reporters to isolate, track the fate or ablate virus-specific *Tcf7*$^{+}$ CD8+ T cells, were transferred into congenically distinct hosts, and the response to acutely resolving LCMV infection was characterized by flow cytometry. The potential of expansion-phase *Tcf7*$^{+}$ and *Tcf7*$^{-}$ CD8^{+} T cell subsets was examined using recall responses in secondary recipient mice while their fate was addressed using *Tcf7*-guided cell tracing and ablation experiments. These findings were related to transcriptome and chromatin accessibility analyses. Group sizes were n=5 or as indicated in the figure legends and experiments were repeated at least twice. Occasional mice were excluded for technical reasons i.e. incomplete i.v. injections.

Mice

C57BL/6 (B6) (CD45.2^{+}) mice were obtained from Envigo (Gannat, France), CD45.1 congenic B6 mice were bred locally, B6 P14 T cell receptor (TCR) transgenic mice (line 237) were provided by H.P. Pircher (Freiburg, Germany) (CD45.2^{+}) (*57*), *Tcf7*$^{-/-}$ mice (*58*) were provided by H. Clevers (Utrecht, The Netherlands). Rosa26 lox stop lox Confetti (*R26*^{Confetti}) (*59*) were provided by J. Joyce (UNIL, Switzerland), Rosa26 lox stop lox TdTomato (*R26*^{Tomato}) (*60*) were provided by J. Huelsken (EPFL, Switzerland), *Tcf7*^{GFP} (*28*), *Tcf7*$^{DTR\text{-}GFP}$ (*31*) and *Tcf7*$^{GFP\text{-}CreERT2}$ (*Tcf7*$^{GFP\text{-}iCre}$) (*22*) mice have been described. P14 *Tcf7*^{GFP}, P14 *Tcf7*^{GFP} *Tcf7*$^{-/-}$, P14 *Tcf7*$^{DTR\text{-}GFP}$, P14 *Tcf7*$^{GFP\text{-}iCre}$ *R26*^{Confetti} and P14 *Tcf7*$^{GFP\text{-}iCre}$ *R26*^{Tomato} mice were obtained by breeding (CD45.2^{+} unless indicated otherwise). Experiments used both male and female mice between 6 and 12 weeks of age, whereby donors and recipients of adoptive T cell transfers were sex matched. Animal experiments were conducted in accordance with protocols approved by the veterinary authorities of the Canton de Vaud (reference numbers VD1124.8 and VD3704).

LCMV infections

Mice were infected with LCMV 53b Armstrong strain (Arm) (2×10^5 plaque forming units (PFU), intraperitoneally (i.p.)), LCMV WE strain (200 PFU, intravenously (i.v.)), LCMV clone 13 (cl13) (200 PFU, i.v.), gp33 epitope mutant (F38L) LCMV cl13 (200 PFU, i.v.) (*38*) or gp33 epitope mutant (A39C) LCMV cl13 (200 PFU, i.v.) (*39*). For recall responses mice were infected with LCMV Arm (2×10^5 PFU, i.p.) or LCMV WE (2000 PFU, i.v.).

Adoptive T cell transfer

P14 cells were obtained by mashing the spleen through a 40 μm nylon cell strainer (BD Falcon). Red blood cells were lysed with a hypotonic Ammonium-Chloride-Potassium (ACK) buffer. $CD8^+$ T cells were purified using mouse $CD8^+$ T cell enrichment kit (StemCell Technologies). Purified P14 cells ($CD45.2^+$ or $CD45.1/2^+$) (usually >95% pure) were adoptively transferred i.v. into naïve B6 ($CD45.2^+$, $CD45.1^+$ or $CD45.1/2^+$) one day prior to infection (d-1). For lineage tracing experiments using *Tcf7*$^{GFP\text{-}iCre}$ *R26*^{Tomato} P14 cells ($CD45.1/2^+$), Tom^- cells were flow sorted and transferred into WT or *Tcf7*$^{GFP\text{-}iCre}$ recipients ($CD45.2^+$). For the analysis of primary responses, the number of P14 input cells depended on the time point of the analysis: ~0.8-2x10^6 P14 cells for analyses at d2 or d3 p.i., 10^5 P14 cells for d4 and 10^4 P14 cells for all later time points. For experiments using KO *Tcf7*^{GFP} cells, $CD62L^+$ *Tcf7*$^{GFP+}$ P14 cells were flow sorted from the spleen of naïve mice before transfer into recipients. For some experiments, purified P14 cells were labelled with CellTrace Violet (CTV; 2.5 μM) according to manufacturer's instructions. For recall responses, 10^4 flow sorted P14 cells were transferred and recipients were infected with LCMV on the same day (d0).

Antibody treatment

For NK cell depletion, mice were injected i.p. with anti-NK1.1 (PK136) (0.5 mg). For IFNAR blockade, mice were injected i.p. with anti-IFNAR1 (MAR1-5A3) (1 mg) or isotype control Ab (mouse IgG1) (MOPC-21). All Abs were purchased from BioXCell.

Tamoxifen (TAM), diphtheria toxin (DT) and EdU treatment

Mice transferred with *R26*^{Tomato} *Tcf7*$^{GFP\text{-}iCre}$ P14 cells were injected i.p. with a single dose of 0.1mg of Tamoxifen (TAM) (T5648, Sigma). Mice transferred with *R26*^{Confetti} *Tcf7*$^{GFP\text{-}iCre}$ P14 cells were injected i.p. with 1 mg of TAM on 3-4 consecutive days. Induction of Cre activity in *R26*^{Confetti} *cells* results in the stochastic and mutually exclusive expression of one of four fluorescent proteins (RFP, CFP, YFP or GFP) (*59*). Herein labeling was followed based on RFP expression. Cre induction also yielded cells expressing high levels of GFP and YFP, which could be discriminated from *Tcf7*$^{GFP\text{-}iCre+}$ cells based on the intermediate GFP levels of the latter. The GFP/YFP^{hi} cells were excluded from the analysis. Control mice were injected with sunflower vehicle only.

Diphtheria Toxin (DT) (D0564, Sigma) was injected i.p. (50 µg/kg of body weight i.e. around 1 µg of DT per mouse). Control mice were injected with PBS.

Mice were injected i.p. with 2mg of 5-ethynyl-2′-deoxyuridine (EdU) 2 h prior to sacrifice.

Cell culture

B6 splenocytes (CD45.1^{+}) were pulsed with gp33-41 peptide (KAVYNFATM) (1µM) for 1h, washed 3 times and used to stimulate P14 cells (CD45.2) purified from the spleen of naive mice. Anti-IL12p40 Ab (1 µg/mL) (C17.8) (BioXcell) and/or IL-12 (0.1–0.3 µg/mL) (Peprotech) or were added as indicated.

P14 cells flow sorted at d2 p.i. (10^4) were cultured for 48-72 h in the presence of naïve splenocytes (10^4) and low dose IL-2 (50 ng/mL) (recombinant human, Glaxo, a gift from N. Rufer, UNIL) to ensure survival. Where indicated IFNβ (1000 U/ml) (Biolegend) was added to the culture.

Vaccination

For DC vaccination, B6 recipient mice (CD45.1^{+} or CD45.1^{+}2^{+}) were adoptively transferred with purified P14 *Tcf7*^{GFP} cells (10^4) (CD45.2^{+}) one day prior to the i.v. injection of bone marrow-derived, LPS-matured and gp33 peptide pulsed DC (DC33) (10^6), with or without i.p. injection of 50 µg of CpG-B 1826 ODNs (TriLink Biotechnologies), as described in detail in (*20*).

For peptide vaccination, purified P14 *Tcf7*^{GFP} cells (10^6) (CD45.2$^+$) were adoptively transferred one day prior to vaccination. Mice were injected s.c. with 50 µg poly(I:C) (Invivogen) together with gp33 peptide (10 µg) (TCMetrix). Mice were analyzed on day 7 post-vaccination.

Tissue preparation and cell suspensions

Spleens were mashed through a 40µM nylon cell strainer to obtain single cell suspensions. This was followed by red blood cells lysis using ACK buffer.

For the isolation of Intraepithelial Lymphocytes (IELs) the small intestine was collected, cut into small pieces and flushed with HBSS 2% FCS, before excising the Peyer's patches. This was followed by incubation with 1mM of Dithiothreitol (DTT) (Applichem, A3668) in HBSS 10% FCS for 20min at 37°C. The cell suspension was filtered using a 100µM strainer (Falcon) and centrifuged and CD8$^+$ T cells were enriched using positive selection by MACS (Miltenyi Biotec kit 130-116-478).

Flow cytometry and cell sorting

Surface staining was performed for 15 min at 4°C in PBS supplemented with 2% FCS (FACS buffer) using the reagents listed in **Data File S4**. For tetramer stainings, cell suspensions were incubated with anti-CD16/32 (2.4G2) hybridoma supernatant before staining for 90min at 4°C with APC-conjugated MHC-I tetramers (**Data File S4)**. Zombie Aqua Fixable Viability kit (Biolegend) was used to exclude dead cells.

For intranuclear staining, cells were surface stained before fixation and permeabilization using the Foxp3 staining kit (eBioscience: Cat. No. 00-5523) followed by intranuclear staining in Permeabilization buffer 1x (Perm buffer).

For cytokine production, splenocytes were re-stimulated *in vitro* with LCMV gp33-41 (gp33) (1µM) peptide for 5h in the presence of Brefeldin A (5µg/ml) for the last 4.5h. Cells were surface stained before fixation and permeabilization (Intracellular Fixation & Permeabilization Buffer Set, eBioscience kit: Cat. No. 88-8824) followed by intracellular staining in 1x Perm buffer. For GzmA

and GzmB detection, splenocytes were cultured in the absence of peptide but in the presence of 5µg/ml of Brefeldin A for 4.5h, before intracellular staining as described above.

EdU was detected with a Click-iT Plus EdU Alexa Fluor 488 Imaging Kit (Molecular Probes, Thermo Fisher Scientific) according to the manufacturer's instructions.

Flow cytometry measurements of cells were performed on an LSR-II or Fortessa flow cytometer (BD). Data were analyzed using FlowJo (TreeStar).

For cell sorting of P14 cells, splenocytes were enriched for $CD8^+$ T cells using the mouse $CD8^+$ T cell enrichment kit (StemCell Technologies) before cell surface staining. Cells were flow sorted to a purity of > 99% (based on post-sort analysis) using a FACSAria (BD) flow cytometer.

Single cell RNA sequencing (scRNAseq) analysis

Purified *Tcf7*^{GFP} P14 cells (CD45.2) were adoptively transferred into B6 (CD45.1) mice prior to infection with LCMV Arm. P14 cells were flow sorted from the spleen of 1 mouse (for d0), pooled spleens of 3 mice (for d2, d3 or d4) or of 2 mice (for d6) and one sample per time point was subjected to scRNAseq analysis as described in **Supplementary Materials and Methods**. After quality control a total of 19,374 cells were retained for further analysis (**Data File S1**). Genes differentially expressed between d0 (T_N) cells and all cells or *Tcf7*$^+$ cells of each time point were identified using the FindMarkers function in Seurat with default parameters and over-representation analyses of the Pathway Interaction Database (PID) (*33*) and Hallmark (*34*) gene set collections from the Molecular Signature Database (MSigDB) v7.5.1) were performed separately for up- or downregulated genes, using the enricher function of the clusterProfiler package (v3.18.1) (*61*).

Gene signatures and calculation of module scores

T_{pCM} and T_{CM} gene signatures derived from bulk RNAseq analysis of d8 *Tcf7*$^+$ (T_{pCM}) versus d8 *Tcf7*$^-$ P14 cells and d30 *Tcf7*$^+$ (T_{CM}) versus d30 *Tcf7*$^-$ P14 cells (T_{EM}) post LCMV Arm infection (*22*). Genes were considered differentially expressed when ($\log_2$(fold change)>2) and are listed in **Data File S2**. A T_{TE} signature was generated using publicly available bulk RNAseq data of Klrg1$^+$

P14 cells (GSM3568611, GSM3568612, GSM3568613) versus Klrg1$^-$ P14 cells (GSM3568614, GSM3568615, GSM3568616) both at d7 post LCMV Arm infection (*47*). Genes were considered differentially expressed when (log_2(fold change)>1.5) (**Data File S2)**. A module score was calculated for each gene signature using the AddModuleScore function in the Seurat package (*62*).

ATACseq analysis

Purified *Tcf7*^{GFP} P14 cells (CD45.2) were adoptively transferred into B6 mice (CD45.1) prior to infection with LCMV Arm. At d4 and d8 p.i., *Tcf7*$^{GFP+}$, *Tcf7*$^{GFP-}$ Klrg1$^-$ and *Tcf7*$^{GFP-}$ Klrg1$^+$ P14 cells were sorted from the spleens of infected recipient mice or from naïve *Tcf7*^{GFP} P14 mice and 3 replicates (5x10^4 cells) of each population were subjected to bulk ATACseq analysis as described in **Supplementary Materials and Methods**. ATACseq peaks were associated to the gene that was closest and located within < 5kb of the gene body. We further incorporated our prior chromatin accessibility data from d28 *Tcf7*$^+$ (T_{CM}) and d28 *Tcf7*$^-$ samples (T_{EM}) (3 replicates each) into the analyses (*22*). The reads overlapping peaks were counted with the dba.count function, followed by normalization and differential accessibility analysis as described above. We transformed the sequencing counts to log_2(counts per million+1) using the cpm function of edgeR (v3.34.1) (*63*), and calculated for each sample the average chromatin accessibility of all peaks associated with a gene.

Data normalization

The number of P14 cells per spleen (output) was re-calculated as if 10^4 cells had been transferred. In addition, for all timepoints, we took into account that the effective take of the transferred cells was 10% (*64*). Output counts are thus normalized to an effective input of 10^4 cells. The fold expansion of P14 cells was also estimated relative to an estimated 10% "take" of the adoptively transferred naïve P14 cells (*64*).

Statistical analyses

Statistical analyses were performed using Prism 8.0 or 9.0 (Graphpad Software). Non-paired *t* test (two-tailed, 95% confidence level) was used for the comparison of 2 data sets. ANOVA was used for >2 comparison groups. *p*-values were considered significant when $p<0.05$, indicated as (*: $p<0.05$; **: $p<0.01$; ***: $p<0.001$; ****: $p<0.0001$); $p>0.05$ was considered non-significant (ns).

Supplementary Materials

Other Supplementary Material for this paper includes the following

References and Notes

1. P. Graef *et al.*, Serial transfer of single-cell-derived immunocompetence reveals stemness of CD8(+) central memory T cells. *Immunity* **41**, 116-126 (2014).
2. A. Lanzavecchia, F. Sallusto, Progressive differentiation and selection of the fittest in the immune response. *Nat Rev Immunol* **2**, 982-987 (2002).
3. S. M. Kaech, W. Cui, Transcriptional control of effector and memory CD8+ T cell differentiation. *Nat Rev Immunol* **12**, 749-761 (2012).
4. A. N. Henning, R. Roychoudhuri, N. P. Restifo, Epigenetic control of CD8(+) T cell differentiation. *Nat Rev Immunol* **18**, 340-356 (2018).
5. V. R. Buchholz, T. N. M. Schumacher, D. H. Busch, T Cell Fate at the Single-Cell Level. *Annu Rev Immunol* **34**, 65-92 (2016).
6. O. Bannard, M. Kraman, D. T. Fearon, Secondary replicative function of CD8+ T cells that had developed an effector phenotype. *Science* **323**, 505-509 (2009).
7. B. Youngblood *et al.*, Effector CD8 T cells dedifferentiate into long-lived memory cells. *Nature* **552**, 404-409 (2017).
8. N. S. Joshi *et al.*, Inflammation directs memory precursor and short-lived effector CD8(+) T cell fates via the graded expression of T-bet transcription factor. *Immunity* **27**, 281-295 (2007).
9. J. T. Chang *et al.*, Asymmetric T lymphocyte division in the initiation of adaptive immune responses. *Science* **315**, 1687-1691 (2007).
10. B. Kakaradov *et al.*, Early transcriptional and epigenetic regulation of CD8+ T cell differentiation revealed by single-cell RNA sequencing. *Nat Immunol* **18**, 422-432 (2017).
11. N. P. Restifo, L. Gattinoni, Lineage relationship of effector and memory T cells. *Curr Opin Immunol* **25**, 556-563 (2013).
12. V. Kalia *et al.*, Prolonged interleukin-2Ralpha expression on virus-specific CD8+ T cells favors terminal-effector differentiation in vivo. *Immunity* **32**, 91-103 (2010).
13. V. P. Badovinac, K. A. Messingham, A. Jabbari, J. S. Haring, J. T. Harty, Accelerated CD8+ T-cell memory and prime-boost response after dendritic-cell vaccination. *Nat Med* **11**, 748-756 (2005).
14. G. R. Starbeck-Miller, H. H. Xue, J. T. Harty, IL-12 and type I interferon prolong the division of activated CD8 T cells by maintaining high-affinity IL-2 signaling in vivo. *J Exp Med* **211**, 105-120 (2014).
15. B. H. Ladle *et al.*, De novo DNA methylation by DNA methyltransferase 3a controls early effector CD8+ T-cell fate decisions following activation. *Proc Natl Acad Sci U S A* **113**, 10631-10636 (2016).
16. S. M. Gray, R. A. Amezquita, T. Guan, S. H. Kleinstein, S. M. Kaech, Polycomb Repressive Complex 2-Mediated Chromatin Repression Guides Effector CD8(+) T Cell Terminal Differentiation and Loss of Multipotency. *Immunity* **46**, 596-608 (2017).
17. L. Pace *et al.*, The epigenetic control of stemness in CD8(+) T cell fate commitment. *Science* **359**, 177-186 (2018).
18. X. Zhou *et al.*, Differentiation and persistence of memory CD8(+) T cells depend on T cell factor 1. *Immunity* **33**, 229-240 (2010).
19. G. Jeannet *et al.*, Essential role of the Wnt pathway effector Tcf-1 for the establishment of functional CD8 T cell memory. *Proc Natl Acad Sci U S A* **107**, 9777-9782 (2010).

20. M. Danilo, V. Chennupati, J. Gomes Silva, S. Siegert, W. Held, Suppression of Tcf1 by inflammatory cytokines facilitates effector CD8 T cell differentiation *Cell Reports* **22**, 2107-2117 (2018).
21. W.-H. W. Lin *et al.*, CD8(+) T Lymphocyte Self-Renewal during Effector Cell Determination. *Cell reports* **17**, 1773-1782 (2016).
22. D. Pais Ferreira *et al.*, Central memory CD8(+) T cells derive from stem-like Tcf7(hi) effector cells in the absence of cytotoxic differentiation. *Immunity* **53**, 985-1000 e1011 (2020).
23. J. J. Obar, L. Lefrancois, Early signals during CD8 T cell priming regulate the generation of central memory cells. *J Immunol* **185**, 263-272 (2010).
24. V. R. Buchholz *et al.*, Disparate Individual Fates Compose Robust CD8(+) T Cell Immunity. *Science* **340**, 630-635 (2013).
25. L. Kretschmer *et al.*, Differential expansion of T central memory precursor and effector subsets is regulated by division speed. *Nat Commun* **11**, (2020).
26. J. B. Johnnidis *et al.*, Inhibitory signaling sustains a distinct early memory CD8(+) T cell precursor that is resistant to DNA damage. *Sci Immunol* **6**, (2021).
27. J. R. Giles *et al.*, Shared and distinct biological circuits in effector, memory and exhausted CD8(+) T cells revealed by temporal single-cell transcriptomics and epigenetics. *Nat Immunol*, (2022).
28. D. T. Utzschneider *et al.*, T Cell Factor 1-Expressing Memory-like CD8(+) T Cells Sustain the Immune Response to Chronic Viral Infections. *Immunity* **45**, 415-427 (2016).
29. N. Sevilla *et al.*, Immunosuppression and resultant viral persistence by specific viral targeting of dendritic cells. *J Exp Med* **192**, 1249-1260 (2000).
30. K. Bresser *et al.*, Replicative history marks transcriptional and functional disparity in the CD8(+) T cell memory pool. *Nat Immunol* **23**, 791-801 (2022).
31. I. Siddiqui *et al.*, Intratumoral Tcf1(+)PD-1(+)CD8(+) T Cells with Stem-like Properties Promote Tumor Control in Response to Vaccination and Checkpoint Blockade Immunotherapy. *Immunity* **50**, 195-211 e110 (2019).
32. A. F. Christiaansen, P. M. Boggiatto, S. M. Varga, Limitations of Foxp3(+) Treg depletion following viral infection in DEREG mice. *Journal of Immunological Methods* **406**, 58-65 (2014).
33. C. F. Schaefer *et al.*, PID: the Pathway Interaction Database. *Nucleic Acids Res* **37**, D674-D679 (2009).
34. A. Liberzon *et al.*, The Molecular Signatures Database (MSigDB) hallmark gene set collection. *Cell Syst* **1**, 417-425 (2015).
35. T. A. E. Elliot *et al.*, Antigen and checkpoint receptor engagement recalibrates T cell receptor signal strength. *Immunity* **54**, 2481-2496 e2486 (2021).
36. D. Zehn, S. Y. Lee, M. J. Bevan, Complete but curtailed T-cell response to very low-affinity antigen. *Nature* **458**, 211-214 (2009).
37. A. C. Richard *et al.*, T cell cytolytic capacity is independent of initial stimulation strength. *Nat Immunol* **19**, 849-858 (2018).
38. S. Johnson *et al.*, Protective efficacy of individual CD8+ T cell specificities in chronic viral infection. *Journal of immunology (Baltimore, Md : 1950)* **194**, 1755-1762 (2015).
39. D. T. Utzschneider *et al.*, High antigen levels induce an exhausted phenotype in a chronic infection without impairing T cell expansion and survival. *The Journal of experimental medicine* **213**, 1819-1834 (2016).

40. M. E. Pipkin *et al.*, Interleukin-2 and inflammation induce distinct transcriptional programs that promote the differentiation of effector cytolytic T cells. *Immunity* **32**, 79-90 (2010).
41. S. J. Keppler, K. Rosenits, T. Koegl, S. Vucikuja, P. Aichele, Signal 3 cytokines as modulators of primary immune responses during infections: the interplay of type I IFN and IL-12 in CD8 T cell responses. *PLoS One* **7**, e40865 (2012).
42. J. Crouse *et al.*, Type I interferons protect T cells against NK cell attack mediated by the activating receptor NCR1. *Immunity* **40**, 961-973 (2014).
43. J. R. Teijaro *et al.*, Persistent LCMV infection is controlled by blockade of type I interferon signaling. *Science* **340**, 207-211 (2013).
44. E. J. Wherry *et al.*, Molecular signature of CD8+ T cell exhaustion during chronic viral infection. *Immunity* **27**, 670-684 (2007).
45. W. Cui, N. S. Joshi, A. Jiang, S. M. Kaech, Effects of Signal 3 during CD8 T cell priming: Bystander production of IL-12 enhances effector T cell expansion but promotes terminal differentiation. *Vaccine* **27**, 2177-2187 (2009).
46. N. Palacio *et al.*, Early type I IFN blockade improves the efficacy of viral vaccines. *J Exp Med* **217**, e20191220 (2020).
47. C. Yao *et al.*, Single-cell RNA-seq reveals TOX as a key regulator of CD8(+) T cell persistence in chronic infection. *Nat Immunol* **20**, 890-901 (2019).
48. P. O. Esteve, U. S. Vishnu, H. G. Chin, S. Pradhan, Visualization and Sequencing of Accessible Chromatin Reveals Cell Cycle and Post-HDAC inhibitor Treatment Dynamics. *Journal of Molecular Biology* **432**, 5304-5321 (2020).
49. S. M. Kaech, R. Ahmed, Memory CD8+ T cell differentiation: initial antigen encounter triggers a developmental program in naive cells. *Nat Immunol* **2**, 415-422 (2001).
50. M. J. B. van Stipdonk, E. E. Lemmens, S. P. Schoenberger, Naive CTLs require a single brief period of antigenic stimulation for clonal expansion and differentiation. *Nat Immunol* **2**, 423-429 (2001).
51. S. Sarkar *et al.*, Functional and genomic profiling of effector CD8 T cell subsets with distinct memory fates. *J Exp Med* **205**, 625-640 (2008).
52. J. P. Scott-Browne *et al.*, Dynamic Changes in Chromatin Accessibility Occur in CD8(+) T Cells Responding to Viral Infection. *Immunity* **45**, 1327-1340 (2016).
53. D. Wang *et al.*, The Transcription Factor Runx3 Establishes Chromatin Accessibility of cis-Regulatory Landscapes that Drive Memory Cytotoxic T Lymphocyte Formation. *Immunity* **48**, 659-674 e656 (2018).
54. R. R. Jadhav *et al.*, Epigenetic signature of PD-1+ TCF1+ CD8 T cells that act as resource cells during chronic viral infection and respond to PD-1 blockade. *Proc Natl Acad Sci U S A* **116**, 14113-14118 (2019).
55. E. Ahn *et al.*, Role of PD-1 during effector CD8 T cell differentiation. *Proceedings of the National Academy of Sciences of the United States of America* **115**, 4749-4754 (2018).
56. M. J. van Stipdonk *et al.*, Dynamic programming of CD8+ T lymphocyte responses. *Nat Immunol* **4**, 361-365 (2003).
57. H. Pircher *et al.*, T cell tolerance to Mlsa encoded antigens in T cell receptor Vb8.1 transgenic mice. *EMBO J.* **8**, 719-727 (1989).
58. S. Verbeek *et al.*, An HMG-box-containing T-cell factor required for thymocyte differentiation. *Nature* **374**, 70-74 (1995).
59. H. J. Snippert *et al.*, Intestinal crypt homeostasis results from neutral competition between symmetrically dividing Lgr5 stem cells. *Cell* **143**, 134-144 (2010).

60. L. Madisen *et al.*, A robust and high-throughput Cre reporting and characterization system for the whole mouse brain. *Nature Neuroscience* **13**, 133-U311 (2010).
61. T. Wu *et al.*, clusterProfiler 4.0: A universal enrichment tool for interpreting omics data. *Innovation (Camb)* **2**, 100141 (2021).
62. I. Tirosh *et al.*, Dissecting the multicellular ecosystem of metastatic melanoma by single-cell RNA-seq. *Science* **352**, 189-196 (2016).
63. M. D. Robinson, D. J. McCarthy, G. K. Smyth, edgeR: a Bioconductor package for differential expression analysis of digital gene expression data. *Bioinformatics* **26**, 139-140 (2010).
64. J. N. Blattman *et al.*, Estimating the precursor frequency of naive antigen-specific CD8 T cells. *J Exp Med* **195**, 657-664 (2002).
65. Y. Hao *et al.*, Integrated analysis of multimodal single-cell data. *Cell* **184**, 3573-3587 e3529 (2021).
66. M. E. Ritchie *et al.*, limma powers differential expression analyses for RNA-sequencing and microarray studies. *Nucleic Acids Res* **43**, e47 (2015).
67. C. W. Law, Y. Chen, W. Shi, G. K. Smyth, voom: Precision weights unlock linear model analysis tools for RNA-seq read counts. *Genome Biol* **15**, R29 (2014).
68. B. Phipson, S. Lee, I. J. Majewski, W. S. Alexander, G. K. Smyth, Robust Hyperparameter Estimation Protects against Hypervariable Genes and Improves Power to Detect Differential Expression. *Ann Appl Stat* **10**, 946-963 (2016).
69. Y. Benjamini, Y. Hochberg, Controlling the false discovery rate: a practical and powerful approach to multiple testing. *Journal of the Royal Statistical Society* **Series B 57** 289–300 (1995).
70. J. D. Buenrostro, B. Wu, H. Y. Chang, W. J. Greenleaf, ATAC-seq: A Method for Assaying Chromatin Accessibility Genome-Wide. *Curr Protoc Mol Biol* **109**, 21 29 21-21 29 29 (2015).
71. J. P. Didion, M. Martin, F. S. Collins, Atropos: specific, sensitive, and speedy trimming of sequencing reads. *Peerj* **5**, e3720 (2017).
72. H. Li *et al.*, The Sequence Alignment/Map format and SAMtools. *Bioinformatics* **25**, 2078-2079 (2009).
73. F. Ramirez *et al.*, deepTools2: a next generation web server for deep-sequencing data analysis. *Nucleic Acids Res* **44**, W160-W165 (2016).
74. A. Tarasov, A. J. Vilella, E. Cuppen, I. J. Nijman, P. Prins, Sambamba: fast processing of NGS alignment formats. *Bioinformatics* **31**, 2032-2034 (2015).
75. Y. Zhang *et al.*, Model-based analysis of ChIP-Seq (MACS). *Genome Biol* **9**, R137 (2008).
76. S. Heinz *et al.*, Simple Combinations of Lineage-Determining Transcription Factors Prime cis-Regulatory Elements Required for Macrophage and B Cell Identities. *Mol Cell* **38**, 576-589 (2010).

Acknowledgments:

We are grateful to D. Speiser and A. Pelletier for critical reading of the manuscript, to C. Fumey for mouse management, the UNIL Flow Cytometry Facility for expert assistance with flow cytometry and the UNIL Genomic Technologies Facility for sequencing analyses.

Funding: This work was supported in part by funding provided by the Swiss National Science Foundation (SNSF) (310030B_179570 and 310030_200898) and the Swiss Cancer Research Foundation (KFS-3601-02-2015 and KFS-5386-08-2021) to W.H.

Author contributions: J.G.S., D.P.F., A.D. and W.H. conceived the study. J.G.S., D.P.F., A.D., T.W., R.V., M.D., M.C. designed and performed experiments, analyzed and interpreted the data. D.D.P contributed valuable virus strains. W.H. acquired funding and supervised the study. D.P.F., A.D., D.D.P. and W.H. wrote original draft and A.D., R.V., M.C. and W.H. revised and edited the manuscript.

Competing interests: D.D.P. is a founder, consultant and shareholder of Hookipa Pharma Inc. commercializing arenavirus-based vector technology, and he is listed as inventor on corresponding patents. The other authors declare that they have no competing interests.

Data and materials availability: Tcf7GFP, Tcf7DTR-GFP and Tcf7GFP-iCre mice are available from Werner Held under a material transfer agreement with the University of Lausanne. RNAseq and ATACseq datasets generated in this study were deposited to the Gene Expression Omnibus database under accession number GEO: GSE221969. All data needed to evaluate the conclusions in the paper are present in the paper or the Supplementary Materials.

Figure Captions:

Figure 1: Presence and stemness of *Tcf7*$^{+}$ CD8^{+} T cells during the primary response to infection

(**A-D**) B6 mice (CD45.1) were adoptively transferred with naïve *Tcf7*^{GFP} P14 cells (CD45.2) and infected with LCMV Arm. P14 cells (CD45.2) were flow sorted on day (d) d0 (naïve, T_N) d2, d3, d4 and d6 post-infection (p.i.) and subjected to scRNAseq analysis. (**A**) Uniform manifold approximation and projection (UMAP) dimensionality reduction of P14 cells analyzed at d0 (T_N) (n=5123), d2 (n=1572), d3 (n=3974), d4 (n=3352) and d6 (n=5353) post-infection. (**B**) UMAP plot of individual P14 cells colored according to their level of expression of a T_{pCM} signature score (genes upregulated in d8 *Tcf7*$^{+}$ (T_{pCM}) versus d8 *Tcf7*$^{-}$ cells). (**C**) Distribution of the T_{pCM} score at the indicated time points of the primary response. The percentage of cells with a T_{pCM} score greater than 0 is shown above each time point. (**D**) UMAP and violin plots showing the distribution of the expression of *Tcf7* (ln(norm. counts+1)) in individual P14 cells and presence of *Tcf7*$^{+}$ cells at distinct time points of the primary response.

(**E-H**) B6 mice (CD45.1/2) were adoptively transferred with *Tcf7*^{GFP} P14 cells (CD45.2) and infected with LCMV Arm. (**E**) Splenic P14 cells were analyzed for *Tcf7*^{GFP} expression at the indicated time points post infection (p.i.). (**F**) Number (N) of *Tcf7*$^{GFP+}$ (green) and *Tcf7*$^{GFP-}$ P14 cells (blue) per spleen, normalized to an input of 10^4 cells. (**G, H**) *Tcf7*$^{GFP+}$ and *Tcf7*$^{GFP-}$ P14 cells (CD45.2) were flow sorted at the indicated time points p.i. and transferred into naïve WT mice (CD45.1 or CD45.1/2) that were infected with LCMV Arm. (**G**) Recipient mice were analyzed 8 days later (dx+8). The bar graph shows the fold expansion of P14 cells compared to input (assuming 10% take). (**H**) Recipient mice were analyzed for the presence of secondary *Tcf7*$^{GFP+}$ P14 cells (green) and the bar graph depicts the fold expansion compared to input (assuming 10% take).

Data shown in (**E-H**) are compiled from 2 experiments with a total of 6-9 mice per time point or group. Data points in (**F, G, H**) represent individual mice. Bar graphs show means (±SD). Statistics in (**G**) is based on multiple unpaired two-tailed Student's test and in (**H**) on two-way ANOVA with Fisher LSD whereby ****: p <0.0001; ***: p<0.001; **: p<0.01; *: p<0.05; and ns (non-significant): p>0.05.

Figure 2: Fate of *Tcf7*$^{+}$ CD8^{+} T cells during the primary response to infection

(**A**) *Tcf7*$^{GFP\text{-}iCre}$ *R26*^{Tom} P14 cells (CD45.2 or CD45.1/2) were adoptively transferred into B6 (CD45.2 or CD45.1/2) or B6 *Tcf7*$^{GFP\text{-}iCre}$ (CD45.2) mice and infected with LCMV WE one day later. Recipient mice were either left untreated (no) or injected with a single dose of Tamoxifen (TAM) on d1 (TAM d1), d2, d3 or d4 p.i.. Gated P14 cells present in the spleen were analyzed for the expression of Tom (*R26*^{Tom}) versus GFP (*Tcf7*$^{GFP\text{-}iCre}$). (**B**) d8 Tom^{+} *Tcf7*$^{GFP\text{-}iCre+}$ cells are highlighted (open green) and d8 Tom^{+} *Tcf7*$^{GFP\text{-}iCre-}$ cells (open blue). (**C, D**) CD62L versus Klrg1 within these subsets at d8. (**E**) d28 Tom^{+} *Tcf7*$^{GFP\text{-}iCre+}$ cells are highlighted (filled green) and d28 Tom^{+} *Tcf7*$^{GFP\text{-}iCre-}$ (filled blue). (**F, G**) CD62L versus Klrg1 within these subsets at d28 p,i. (**H**) The number (N) of Tom^{+} *Tcf7*$^{GFP\text{-}iCre+}$ cells at d8 compared to d28 p.i. (**I**) The number of Tom^{+} *Tcf7*$^{GFP\text{-}iCre+}$ compared to Tom^{+} *Tcf7*$^{GFP\text{-}iCre-}$ cells at d28. (**J**) The number of Tom^{+} *Tcf7*$^{GFP\text{-}iCre-}$ cells at d8 compared to d28 p.i. Data in (**B-J**) are compiled from 3 independent experiments with a total of n=6-9 mice per group. Data points in (**H-J**) represent individual mice. Bar graphs show means (±SD). Statistics in (**H-J**) is based on two-way ANOVA with Fisher LSD test whereby ****: p <0.0001; ***: p<0.001; **: p<0.01; *: p<0.05; and ns (non-significant): p>0.05.

Figure 3: Progressively limited differentiation of *Tcf7*$^{+}$ CD8^{+} T cells during the primary immune response

(**A**) *Tcf7*^{GFP} P14 cells (10^4) (CD45.2) were transferred into B6 mice (CD45.1/2) and infected with LCMV Arm on the same day (P14 transfer d0). Alternatively, recipient mice were infected 3 days prior to the transfer of *Tcf7*^{GFP} P14 cells (P14 transfer d3) Recipient mice were analyzed on d8 p.i. for (**B**) the number of P14 cells and (**C**) the number of *Tcf7*$^{GFP+}$, *Tcf7*$^{GFP-}$ and *Tcf7*$^{GFP-}$ Klrg1^{+} P14 cells. (**D**) B6 mice (CD45.1/.2) were transferred with *Tcf7*$^{DTR\text{-}GFP}$ or *Tcf7*^{GFP} P14 cells (CD45.2) and infected with LCMV Arm one day later. Recipient mice were injected with Diphtheria Toxin (DT) on d4 and d5 p.i. Gated P14 cells were analyzed for the numbers of GFP^{+} (*Tcf7*$^{DTR\text{-}GFP+}$ or control *Tcf7*$^{GFP+}$) cells on (**E**) d6, (**F**) d8 or (**G**) d16 p.i.. (**H**) P14 cells were analyzed for the expression of CD62L versus Klrg1 at d16 p.i. The bar graphs show the numbers of CD62L^{+} Klrg1^{-} P14 cells at d16 p.i. (**I**) The bar graphs show the numbers of IL-2^{+} P14 cells at d16 p.i.. (**J**) Numbers

of GFP$^+$ (*Tcf7*$^{DTR\text{-}GFP+}$ or control *Tcf7*$^{GFP+}$) P14 cells on d6, d8 and d16 p.i.. Data in (**A-C**) are compiled from 2 independent experiments with a total of n=8 mice per group. Data in (**D-J**) are compiled from 2 independent experiments with a total of n=5-12 mice per group. Data points in (**B, C, E-J**) represent individual mice. Bar graphs show means (±SD). Statistics is based on unpaired 2-tailed student's t-test (**B, C, E-I**) or One-Way ANOVA with Fisher's LSD test (**J**) whereby ****: p <0.0001; ***: p<0.001; **: p<0.01; *: p<0.05; and ns (non-significant): p>0.05.

Figure 4: Low TCR input disfavors T_{TE} relative to T_{pCM} formation

(**A**) Genes differentially expressed between T_N and *Tcf7*$^+$ or *Tcf7*$^-$ cells present at the different time points of infection (based on the scRNAseq analysis) were subjected to over-representation analysis using the Pathway Interaction Database (PID) and the Hallmark (H) gene set collections. The graph shows the significance (-$\log_{10}$ of adjusted p-values) for the indicated gene sets. For graphical representation, the -$\log_{10}$(adj. p-value) of gene sets down-regulated in *Tcf7*$^+$ or *Tcf7*$^-$ cells versus T_N cells was multiplied by -1. The dotted line depicts the limit of statistical significance (i.e. ±$\log_{10}$(0.05)). (**B**) B6 mice (CD45.1/2) were adoptively transferred with naïve *Tcf7*^{GFP} P14 cells (CD45.2) and infected with a fixed but low dose of wild-type (WT) and Δgp33 (F38L) LCMV cl13, whose gp33 epitope has no measurable affinity for the P14 TCR. The mixtures ranged from 100%, 30%, 10%, 3% to 0% of WT virus. (**C**) Number of P14 cells and (**D**) of *Tcf7*$^{GFP+}$ and *Tcf7*$^{GFP-}$ P14 cells at d8 p.i. (**E-H**) B6 mice (CD45.1 or CD45.1/2) were adoptively transferred with naïve *Tcf7*^{GFP} P14 cells (CD45.2) and infected with a fixed low dose of WT, F38L (Δgp33) or A39C LCMV cl13, whose gp33 epitope has a low affinity for the P14 TCR. (**E**) Number of P14 cells and (**F**) frequency and number of *Tcf7*$^{GFP+}$ and *Tcf7*$^{GFP-}$ P14 cells at d8 p.i. (**G, H**) Gated *Tcf7*$^{GFP+}$ and *Tcf7*$^{GFP-}$ cells were analysed for (**G**) CD62L versus Klrg1 expression or (**H**) IL-2 versus IFNγ production. The data in (**B-H**) are compiled from 2 independent experiments with a total of n=7-8 mice per group. Data in (**H**) are from a single experiment with of n=4 mice per group. Data points in (**C-H**) represent individual mice. Means (±SD) are shown. Statistics are based on One-Way ANOVA with Fisher's LSD test (**C-E, G, H**) or non-paired two-tailed Student's test (**F**) with ****: p <0.0001; ***: p<0.001; **: p<0.01; *: p<0.05; and ns (non-significant): p>0.05.

Figure 5: Inflammatory signaling is dispensable for T_{pCM} formation

(**A-D**) B6 mice (CD45.1/2) were adoptively transferred with naïve *Tcf7*^{GFP} P14 cells (CD45.2) and infected with LCMV Arm one day later (d0). Recipient mice were treated with anti-NK1.1 (to deplete NK cells) and anti-IFNAR or isotype control Ab at d-1. (**A**) Number of P14 cells and (**B**) frequency and number of *Tcf7*$^{GFP+}$, *Tcf7*$^{GFP-}$ and *Tcf7*$^{GFP-}$ Klrg1^{+} P14 cells at d8 p.i.. (**C, D**) Gated *Tcf7*$^{GFP+}$ and *Tcf7*$^{GFP-}$ cells were analyzed for (**C**) CD62L versus Klrg1 expression or (**D**) IL-2 versus IFNγ production. (**E-H**) B6 mice (CD45.1) adoptively transferred with *Tcf7*^{GFP} P14 cells (10^4) (CD45.2) were vaccinated with LPS-matured and gp33 peptide pulsed DC (DC33) without or with TLR9 ligand CpG-B (DC33+CpG). (**E**) Number of P14 cells and the frequency and number of (**F**) *Tcf7*$^{GFP+}$, *Tcf7*$^{GFP-}$ and *Tcf7*$^{GFP-}$Klrg1^{+} P14 cells at d7 post vaccination. (**G, H**) Gated *Tcf7*$^{GFP+}$ and *Tcf7*$^{GFP-}$ cells were analysed for (**G**) CD62L versus KLRG1 expression or (**H**) IL-2 versus IFNγ production. Data in (**A-C**) are compiled from 2 independent experiments with a total of n= 5 mice per group. Data in (**D**) are from a single experiment with n= 4 mice per group. Data in (**E-H**) are from one experiment of 2 performed, each with n=3-5 mice per group. Data points in (**A-H**) represent individual mice. Means (±SD) are shown. Statistics are based on non-paired two-tailed Student's test (**A, B, E, F**) or One-Way ANOVA with Fisher's LSD test (**C, D, G, H**) with ****: p <0.0001; ***: p<0.001; **: p<0.01; *: p<0.05; and ns (non-significant): p>0.05.

Figure 6: Role of priming and inflammatory signals in CD8^{+} T cell cycling and TCF1 downregulation

(**A, B**) B6 mice (CD45.1) were depleted of NK cells, treated with isotype control or anti-IFNAR, transferred with CTV-labelled P14 cells (CD45.2) (10^6) and infected with LCMV WE. (**A**) Frequency of P14 cells on d3.5 p.i.. (**B**) Gated P14 cells were analysed for CTV versus TCF1, discriminating between undivided TCF1^{+} cells, low divided TCF1^{+} cells (1-3 divisions), high divided TCF1^{+} cells (>3 divisions) and high divided TCF1^{-} cells (>3 divisions). The bar graphs show the fraction of undivided TCF1^{+} cells (left) and the ratio of TCF1^{+} versus TCF1^{-} cells that had divided >3 times (right). (**C-F**) B6 mice (CD45.1) were treated with anti-IFNAR, transferred with CTV-labelled P14 cells (CD45.2) (10^6) and infected with LCMV WE on d0. Undivided P14

cells were flow sorted on d2 p.i. and cultured *in vitro* in the presence or absence of IFNβ for 2-3 days. (**D, E**) Gated P14 cells were analysed for CTV versus TCF1. Gates discriminate between undivided TCF1$^+$ cells, divided TCF1$^+$ cells and divided TCF1$^-$ cells. (**F**) Fraction of undivided TCF1$^+$ cells (left), divided TCF1$^+$ cells and divided TCF1$^-$ cells from (**D and E).** (**G-J**) B6 mice (CD45.1) were transferred with CTV-labelled WT or *Tcf7* KO *Tcf7*^{GFP} P14 cells (CD45.2) (10^6) and infected with LCMV WE. (**G**) Frequency of P14 cells on d3.5 p.i.. Gated P14 cells were analysed for (**H**) TCF1 and (**I**) CTV versus *Tcf7*^{GFP}. (**J**) Gated *Tcf7*$^{GFP+}$ and *Tcf7*$^{GFP-}$ cells were analysed for CTV. Gates distinguish between undivided, divided (1-3 divisions) and highly divided cells (>3 divisions), with the frequencies of highly divided cells in each subpopulation shown in graphs alongside.

(**A, B**) Data are compiled from 3 independent experiments with a total of n=6-7 mice per group. (**C-F** and **G-J**) Data are compiled from 2 independent experiments with a total of n=3-6 mice per group. Data points in (**A, B, G, J**) represent individual mice or (**F)** cultures derived from individual mice. Means (±SD) are shown. Statistics are based on non-paired two-tailed Student's test (**A**, **B, G, J**) and One-Way ANOVA with Fisher's LSD test (**F**) with ****: p <0.0001; ***: p<0.001; **: p<0.01; *: p<0.05; and ns (non-significant): p>0.05.

Figure 7: Stable loss of the T_{pCM} gene signature occurs upon *Tcf7* downregulation and precedes stable acquisition of a T_{TE} gene signature

B6 mice (CD45.1) were adoptively transferred with naïve *Tcf7*^{GFP} P14 cells (CD45.2) and infected with LCMV Arm. (**A-C**) P14 cells (CD45.2) cells were flow sorted on d2, d3, d4 and d6 post-infection p.i. and, together with naïve P14 cells (T_N), subjected to scRNAseq. (**A**) UMAP plot of P14 cells colored according to the time point p.i. (left) (described in Fig. 1A), and according to their T_{TE} signature score (right), derived as described in Materials and Methods. (**B**) Expression of selected T_{TE} genes (ln(norm. counts+1)) by individual P14 cells. (**C**) Individual P14 cells colored according to the time point p.i. (described in Fig. 1A), were analyzed for the overall intensity of the T_{TE} versus the T_{pCM} signature score. (**D-I**) *Tcf7*$^{GFP+}$, *Tcf7*$^{GFP-}$ Klrg1$^-$ and *Tcf7*$^{GFP-}$ Klrg1$^+$ P14 cells (CD45.2) were flow sorted on d4 or d8 p.i. and, together with naïve P14 cells (T_N) and prior data from d28 *Tcf7*$^+$ and d28 *Tcf7*$^-$ memory cells, subjected to bulk ATACseq analysis. (**D**) A total of n=323 genes are overexpressed and more accessible in T_{pCM} (d8 *Tcf7*$^+$ compared to d8 *Tcf7*$^-$

cells) and n=56 genes are overexpressed and more accessible in T_{TE} (d8 *Tcf7*$^{-}$ Klrg1^{+} compared to d8 *Tcf7*$^{+}$ cells). The bar graph shows the number of overexpressed and more accessible T_{pCM} signature genes (yellow bars) or T_{TE} signature genes (purple bars) in the indicated populations of *Tcf7*$^{+}$ and *Tcf7*$^{-}$ cells. (**E**) The epigenetically regulated T_{pCM} signature genes (n=323) were associated with n=876 more accessible regions. The box plot depicts the average read coverage for these regions in the indicated populations of cells. (**F, I**) Genome browser view of sequencing read coverage (dark blue tracks) at the *Tcf7* (**F**) and GzmB locus (**I**). Black horizontal lines depict accessible regions based on peak calling. The dot graphs in (**F, I**) depict means (±SD) of the normalized accessibility of the called peak overlapping the transcriptional start site (TSS) in the different populations (n=3 samples).

(**G**) Motif search analysis of regions more accessible in T_{pCM} genes (excluding repetitive regions).

(**H**) The epigenetically regulated T_{TE} genes (n=56) were associated with n=152 more accessible regions. The box plot depicts the average read coverage for these regions in the indicated populations of cells.

Statistics in (**F, I**) is based on One-Way ANOVA with Fisher's LSD test with ****: p <0.0001; ***: p<0.001; **: p<0.01; *: p<0.05; and ns (non-significant): p>0.05.

SUPPLEMENTARY MATERIALS

This PDF file includes:

Other Supplementary Material for this paper includes the following

SUPPLEMENTARY METHODS

Single cell RNA sequencing (scRNAseq) analysis

Cell droplet encapsulation, lysis and RNA capture was performed using 10x Chromium Controller (10x Genomics) and the Chromium Single Cell 3′ v3 Reagent Kit according to the manufacturer's protocol. One cDNA library per time point post infection was generated and further sequenced (paired-end) on a HiSeq4000 device (Ilumina) at the Lausanne Genomic Technologies Facility (https://wp.unil.ch/gtf/).

The raw sequencing reads were filtered, demultiplexed and aligned to the mouse genome and transcriptome (mm10, refdata-gex-mm10-2020-A) using the 10x Genomics Cell Ranger pipeline (version 5.0.1). The cellranger count function was used with default parameters (i.e. --include-introns=FALSE), except for d4 cells where the parameter --force-cells=3399 was provided. A total of 20169 cells were called by the Cell Ranger pipeline (**Data file S1**). Downstream analyses were performed in R (v4.0.2) using the Seurat package (v4.0.4) (*65*) for most analyses. We imported the filtered feature x barcode matrices into R, and retained cells that had between 1000 and 5000 detected genes, as well as less than 20% of mitochondrial gene expression, resulting in 19374 cells retained (**Data file S1**).

Gene counts were converted to ln(normalized counts+1) by using the NormalizeData function of the Seurat package, with parameters normalization.method="LogNormalize" and scale.factor=10000. The data was then scaled, and a principal component analysis was performed using the 2000 most variable genes selected by the variance stabilizing (vst) detection method. Cells were projected into a reduced dimension space by using the Uniform Manifold Approximation and Projection (UMAP) on the 20 first principal components.

Differential gene expression analysis between cells originating from different time points was performed using the FindMarkers function in Seurat with default parameters. We determined differentially expressed (DE) genes of all cells of each time point against d0 (T_N) cells, or between *Tcf7*$^+$ cells of each time point against *Tcf7*$^+$ d0 (T_N) cells. For functional analysis of DE genes, over-representation analyses of the Pathway Interaction Database (PID) (*33*); and Hallmark (*34*) gene set collections (downloaded from The Molecular Signature Database (MSigDB) v7.5.1) were

performed separately for up- or downregulated genes of each time point, using the enricher function of the clusterProfiler package (v3.18.1) (*61*).

Definition of gene signatures and calculation of module scores

We defined gene signatures to determine whether or not these signatures were expressed in any of the single cells that we profiled by scRNAseq. First, the Klrg1$^+$ short lived effector signature was generated by re-processing raw bulk RNA sequencing data available in the Gene Expression Omnibus (GEO) database, accession number GSE119942 (*47*). We downloaded fastq files for three samples of Klrg1$^+$ cells (P14 d7 p.i. Arm, accession numbers: GSM3568611, GSM3568612, GSM3568613) and three samples of Klrg1$^-$ cells (P14 d7 p.i. Arm, acc. numbers: GSM3568614, GSM3568615, GSM3568616). Raw sequencing reads were aligned to the mouse genome (mm10) using the bcbio-nextgen pipeline (v1.2.4). In this pipeline, reads were aligned with HISAT2 (v2.2.1), and counts were summarized at the gene level with featureCounts (v2.0.1). Raw counts were imported into R and genes expressed at more than at 1 count per million (cpm) in at least one sample were retained (n=15598 retained genes). Normalization factors were calculated using the trimmed mean of M-values (TMM) method implemented in edgeR (v3.24.3) (*63*), and counts were converted to $\log_2$(cpm) using the voom function implemented in limma (v3.46.0) (*66*) (*67*). Genes differentially expressed between Klrg1$^+$ short lived effector cells and Klrg1$^-$ memory precursor cells were determined by fitting a linear model to the normalized gene expression data followed by empirical Bayes moderation using the functions lmFit and eBayes (*68*) implemented in the limma package. P-values were adjusted using the Benjamini-Hochberg procedure (*69*). The Klrg1$^+$ short lived effector gene signature contained 54 genes that were upregulated and had $\log_2$(fold change)>1.5. The Klrg1$^-$ memory precursor gene signature contained 248 genes that were downregulated and had $\log_2$(fold change) <1.5 (**Data file S2**).

T_{pCM} and T_{CM} gene signatures derived from differential gene expression analysis that have been reported in (*22*). In brief, Pais Ferreira et al. sorted *Tcf7*$^+$ and *Tcf7*$^-$ P14 cells at d8 p.i. or at d30 post LCMV Arm infection. These 4 cell populations were subjected to bulk RNA sequencing and differentially expressed genes were obtained. The T_{pCM} gene signature contained 198 genes that were upregulated in d8 *Tcf7*$^+$ versus d8 *Tcf7*$^-$ P14 cells and had a $\log_2$(fold change)>2. The d8 *Tcf7*$^-$ signature contained 236 genes downregulated ($\log_2$(fold change)<2) in d8 *Tcf7*$^+$ versus d8 *Tcf7*$^-$ P14 cells. The T_{CM} gene signature contained 43 genes that were upregulated in d30 *Tcf7*$^+$

versus d30 *Tcf7*$^{-}$ P14 cells and had a $\log_2$(fold change)>2. Finally, the T_{EM} gene signature contained 103 genes that were downregulated in d30 *Tcf7*$^{+}$ versus d30 *Tcf7*$^{-}$ P14 cells and had a $\log_2$(fold change)<2. All genes are listed in **Data file S2**. The module score for each gene signature was calculated using the AddModuleScore function implemented in the Seurat package (*62*).

ATACseq analysis

Purified *Tcf7*^{GFP} P14 cells (CD45.2) were adoptively transferred into B6 mice (CD45.1) prior to infection with LCMV Arm. At d4 and d8 p.i., *Tcf7*$^{GFP+}$, *Tcf7*$^{GFP-}$ Klrg1^{-} and *Tcf7*$^{GFP-}$ Klrg1^{+} P14 cells were sorted from the spleens of infected recipient mice or from naïve *Tcf7*^{GFP} P14 mice and subjected to bulk ATACseq analysis.

ATAC-seq was performed as described (*70*). Briefly, 5x10^4 flow sorted CD8^{+} T cells were washed with cold 1x PBS and resuspended in 50 µl of ice-cold lysis buffer (10mM Tris-Cl, pH 7.4, 10nM NaCl, 3mM $MgCl_2$ and 0.1% (v/v) of NP-40. Cells were centrifuged immediately and the resulting pellet (nuclei) was resuspended in 50 µl of transposase reaction mix (25 µl 2xTD buffer (Illumina), 25 µl Tn5 transposase (Illumina) and 22.5 µl of nuclease-free water), followed by incubation at 37ºC for 30 min (while gently shacking). Tagmented DNA was cleaned using QIAGEN MinElute PCR Purification kit as described in the kit's protocol. Library preparation was performed using Illumina's Unique Dual (UD) Indexes (R#20027213) and NEBNext High-Fidelity 2x PCR Master Mix (M0541), using the following program: 5 min 72ºC, 30s 98ºC; 10 cycles: 10s 98ºC, 30s 63ºC, 1 min 72ºC: Hold 4ºC. The sequencing libraries were sequenced on 4 lanes of an Illumina HiSeq 4000 device (paired-end, 150 read length) at the Lausanne Genomic Technologies Facility.

For each file, the fastq files of the 4 separate lanes were concatenated into a single fastq file. The sequencing files were processed using the "atac" method of the bcbio-nextgen pipeline (v1.2.4). The pipeline first started by trimming sequencing adapters (Illumina and TruSeq) and low quality ends using Atropos (v1.1.28) (*71*), with arguments --overlap 8, --minimum-length 25, --quality-cutoff 5 and --no-default-adapters. The quality-filtered and trimmed reads were aligned to the mouse genome (mm10, 2018-10-10 94) using the bwa mem algorithm (v0.7.17-r1188) (https://arxiv.org/abs/1303.3997), with arguments -c 250 and -M. Sequence alignment map (sam) files were sorted and converted to binary (bam) files using biobambam2 (v2.0.87) (https://gitlab.com/german.tischler/biobambam2) and indexed using samtools (v1.9) (*72*). To correct for the 9-bp duplication created by DNA repair of the nick by the Tn5 transposase, the

aligned reads were shifted using alignmentSieve (deepTools3 v3.5.0) (*73*) with the --ATACshift and --minMappingQuality arguments. Samtools and sambamba (v0.7.1) (*74*) were used with the shifted aligned reads as input to remove reads aligning to the mitochondrial genome, unmapped reads or reads not forming proper pairs, as well as duplicate reads. Finally, using the bam files of the 3 replicates per cell population, peaks of accessible chromatin were called using the callpeak function of Macs2 (v2.2.7.1) (*75*), with arguments -g 'mm', --keep-dup all, --broad and -q 0.05.

Subsequent analyses were performed with R (v4.1.0). ATACseq peaks were called were called using the callpeak function of Macs2 (v2.2.7.1) (*75*). The reads overlapping peaks called by Macs2 were counted using the dba.count function of the DiffBind package (v3.2.7), with arguments minOverlap=2, score=DBA_SCORE_NORMALIZED, bSubControl=F, summits=0 and filter=1. Differential chromatin accessibility analysis between all pairs of cell populations was performed with the dba.analyze function, with method=DBA_ALL_METHODS, and significant peaks were extracted using the dba.report function with method=DBA_DESEQ2. Peaks were annotated to neighboring genes (annotation for mm10: GRCm38.p1) using the function annotatePeakInBatch of the ChIPpeakAnno package (v3.26.4). Each peak was associated to the gene that was the closest from the middle of the peak, retaining peaks that were located within ± 5kb of the gene body.

Finally, we determined whether regions associated with genes significantly differentially expressed between T_{pCM} versus T_{TE} or between T_{CM} versus T_{EM} (RNAseq reported in (*22*)) had different chromatin accessibility in each of the different CD8 T cell populations. To this end, we transformed the sequencing counts to $\log_2$(counts per million+1) using the cpm function of edgeR (v3.34.1) (*63*), and calculated for each sample the average chromatin accessibility of all peaks associated with significantly differentially expressed genes.

Our analyses included chromatin accessibility data from T_{CM} and T_{EM} cells (Pais Ferreira *et al*., 2020). The bam files of d28 *Tcf7*$^{+}$ (T_{CM}) and d28 *Tcf7*$^{-}$ samples (T_{EM}) (3 replicates each) were combined with the ones from the different populations and time points described here, and the reads overlapping peaks were counted with the dba.count function, followed by normalization and differential accessibility analysis as described above.

Genomic regions associated with genes differentially expressed either in T_{pCM}, T_{TE} or T_{CM} were subjected to enrichment analysis of transcription factor binding site motifs using the Homer software (v. 4.11) (*76*). The perl script findMotifsGenome.pl was used with the following parameters: mm10, -mask, -size=given and -mset=vertebrates. We performed motif enrichment

analysis either on the more accessible or on the less accessible genomic regions separately. Based on motif similarity, Homer matched the *de novo* motifs to the best transcription factor, and we discarded the ones labeled as being possible false positives.

SUPPLEMENTARY FIGURES

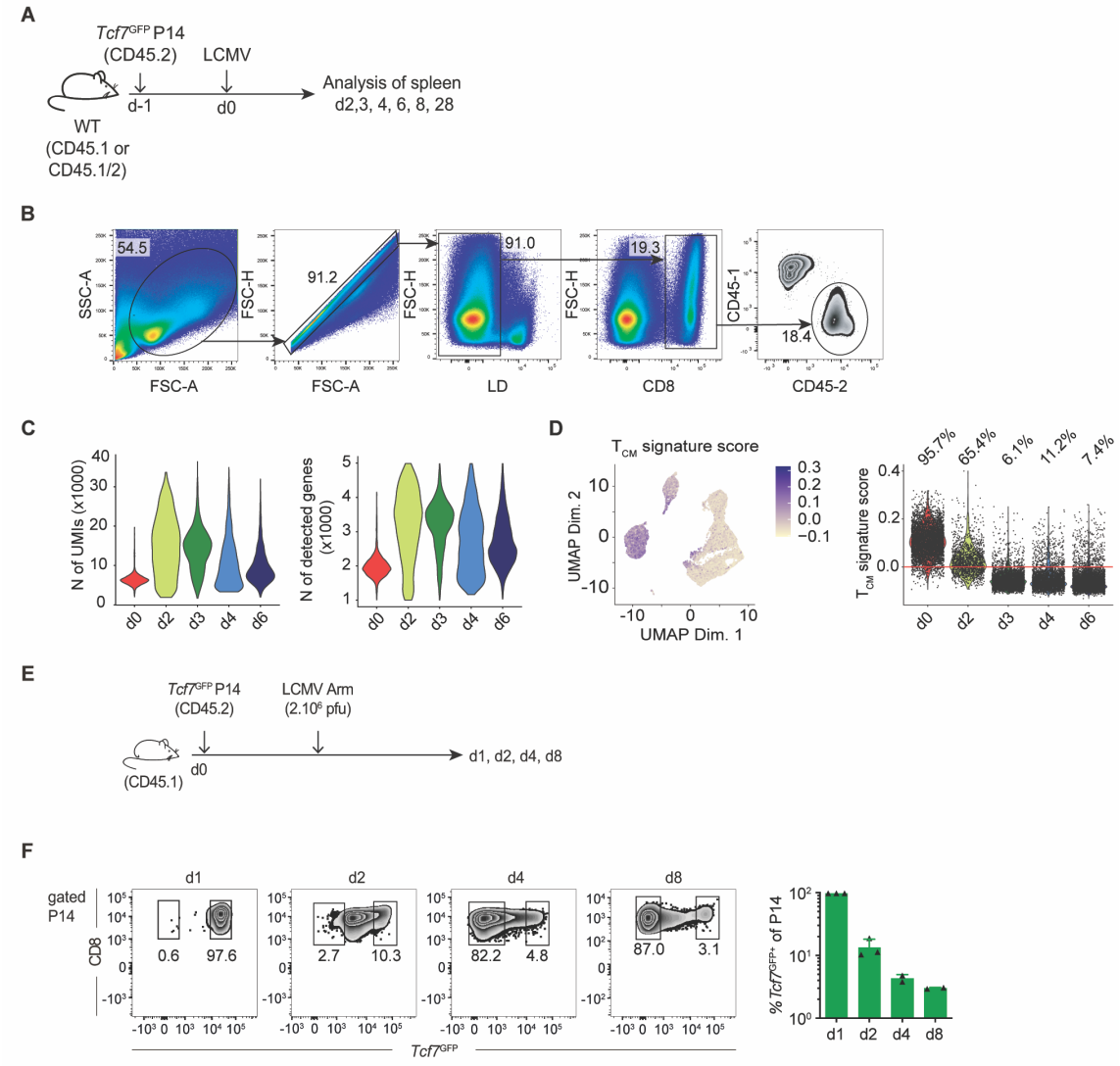

Fig. S1: Presence of *Tcf7*⁺ CD8⁺ T cells during the primary response to infection

(**A**) Experimental schematic: Naïve P14 cells (CD45.2) were transferred into congenically distinct B6 mice (CD45.1) that were subsequently infected with LCMV (Arm or WE strain). On the indicated day of infection, P14 cells present in the spleen (unless indicated otherwise) were characterized using flow cytometry. (**B**) Live cells were gated using FSC-A and SSC.A, followed by doublet discrimination using FSC-H/FSC-A. Next, singlets were gated for alive cells, CD8⁺ and congenic markers CD45.1 and CD45.2 were used to gate P14 cells.

(**C, D**) B6 mice (CD45.1) were adoptively transferred with naïve *Tcf7*^{GFP} P14 cells (CD45.2) and infected with LCMV Arm. P14 cells (CD45.2) cells were flow sorted on d0 (naïve cells T_N), d2, d3, d4 and d6 post-infection (p.i.) and subjected to scRNAseq analysis. (**C**) Number of unique molecular identifiers (UMIs) (left) and number of detected genes (right) per time point p.i.. (**D**) UMAP plot of individual P14 cells colored according to their expression level of genes differentially expressed in d30 *Tcf7*$^{+}$ cells (upregulated genes = T_{CM} signature score) versus d30 *Tcf7*$^{-}$ cells (*22*). The UMAP plot of the T_{CM} score is split by the distinct time points post infection. Distribution of the T_{CM} score in individual P14 cells at the indicated time points post infection. The percentage of cells with a T_{CM} signature score greater than 0 is shown above each time point. (**E**) Naïve *Tcf7*^{GFP} P14 cells (CD45.2) were transferred into B6 mice (CD45.1) that were subsequently infected with a high dose ($2x10^6$ pfu) of LCMV Arm. (**F**) At the indicated time point p.i., gated P14 cells present in the spleen were analyzed for *Tcf7*^{GFP} expression.

Data in (**F**) are from a single experiment with n=2-3 mice per time point. Data points in (**F**) represent individual mice. Means (±SD) are shown.

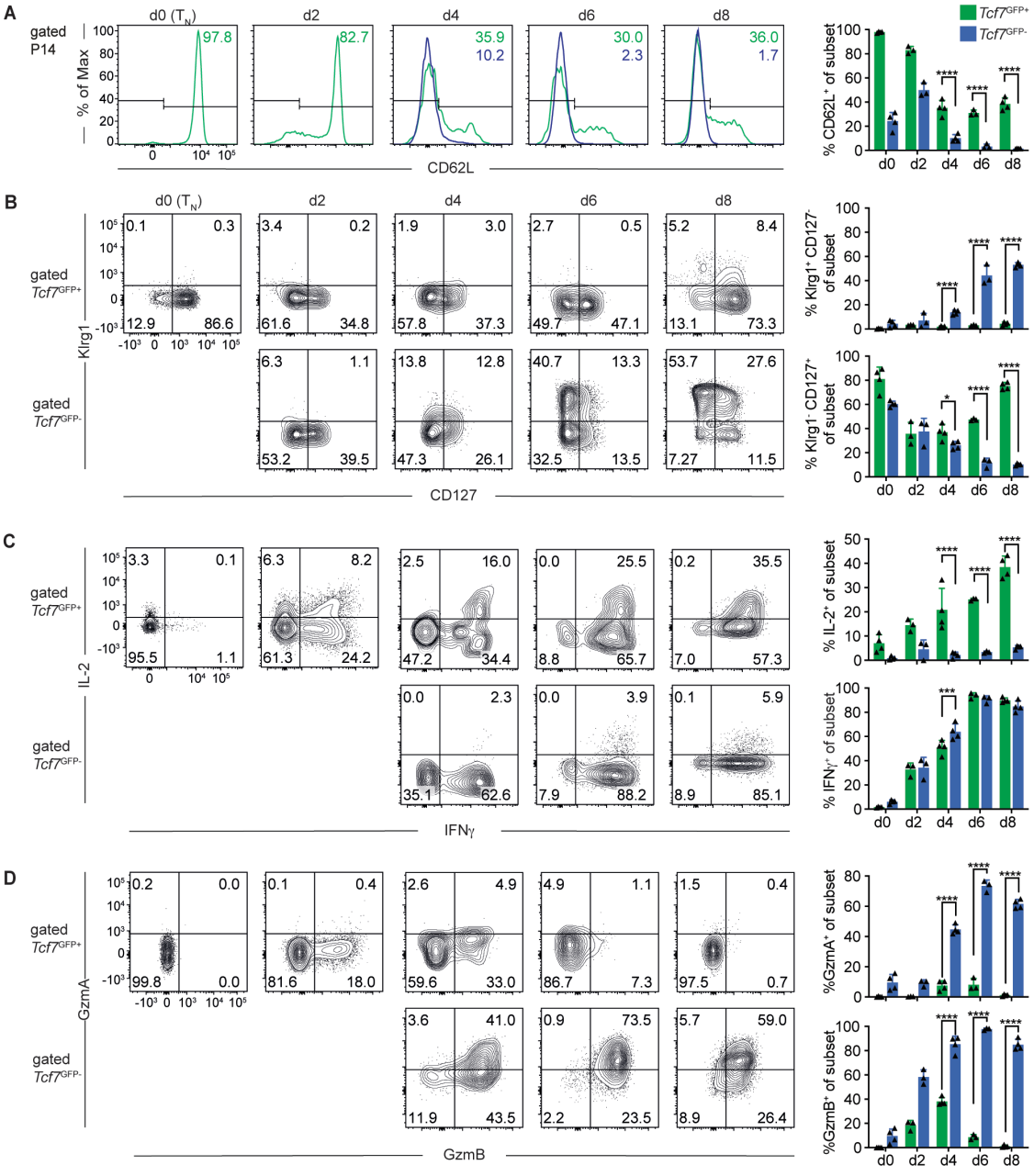

Fig. S2: Phenotype of *Tcf7*$^{+}$ CD8^{+} T cells during the primary response to infection

(**A-D**) B6 (CD45.1/2) mice were adoptively transferred with *Tcf7*^{GFP} P14 cells (CD45.2) (2x10^{6} cells for d2, 10^{5} cells for d4 and 10^{4} cells for d6 and d8) and infected with LCMV WE. At the indicated time points p.i. gated *Tcf7*$^{GFP+}$ and *Tcf7*$^{GFP-}$ P14 cells (see Fig. 1E) were analyzed for (**A**) CD62L expression, (**B**) CD127 versus Klrg1 expression (**C**) the production of IL-2 and IFNγ in

response to *in vitro* restimulation with gp33 peptide and (**D**) the expression of GzmA and GzmB. Data in (**A-C**) are representative of 2 independent experiments each with n=3-5 mice per time point and data in (**D**) derive from 1 experiment with n=3-4 mice per time point. Data points in (**A-D**) represent individual mice. Means (±SD) are shown and statistics are based on Two-way ANOVA with Fisher's LSD test with *: $p<0.05$; ***: $p<0.001$; ****: $p<0.0001$ and (ns) $p>0.05$.

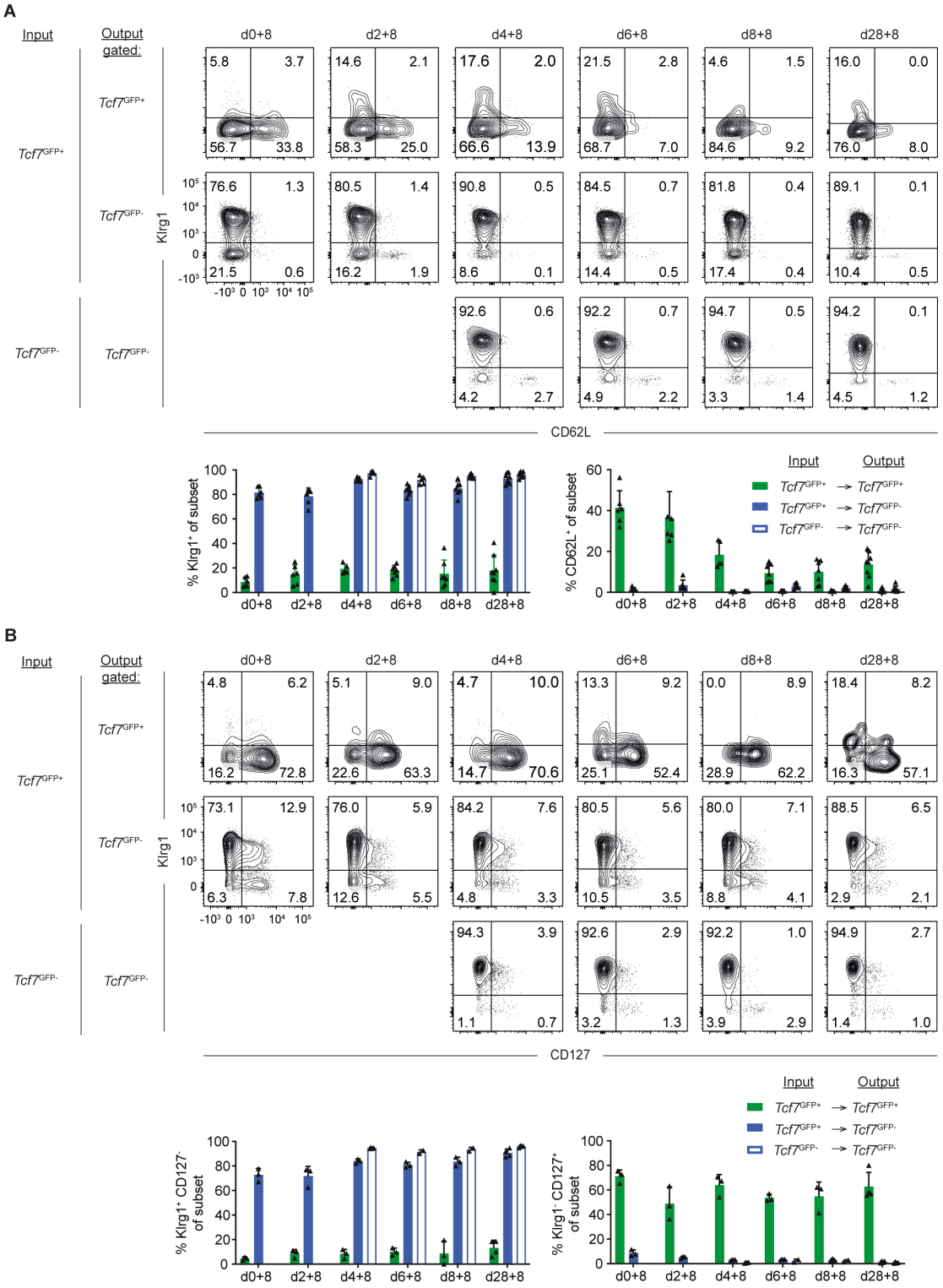
A
Input
Output gated:
d0+8
d2+8
d4+8
d6+8
d8+8
d28+8
Tcf7GFP+
Tcf7GFP-
Klrg1
CD62L
% Klrg1+ of subset
% CD62L+ of subset
Input
Output
B
CD127
% Klrg1+ CD127- of subset
% Klrg1- CD127+ of subset

Fig. S3: Stemness of *Tcf7*$^{+}$ CD8^{+} T cells during the primary response to infection

B6 mice (CD45.1/2) were adoptively transferred with *Tcf7*^{GFP} P14 cells (CD45.2) and infected with LCMV Arm. At the indicated time points p.i., splenic *Tcf7*$^{GFP+}$ or *Tcf7*$^{GFP-}$ P14 cells were sorted and transferred into secondary B6 recipients that were then infected with LCMV Arm. The secondary recipients were analyzed 8 days later (dx+8). Gated secondary *Tcf7*$^{GFP+}$ or *Tcf7*$^{GFP-}$ P14 cells were analyzed for the expression of (**A**) CD62L versus Klrg1 and (**B**) CD127 versus Klrg1. The bar graphs show the percentage of positive cells in the indicated subset.

Data shown in (**A**) are compiled from 2 experiments with a total of 6-8 mice per group, data in (**B**) are from one representative experiment of 2 performed each with 3-4 mice per group. Data points in (**A, B**) represent individual mice. Bar graphs show means (±SD).

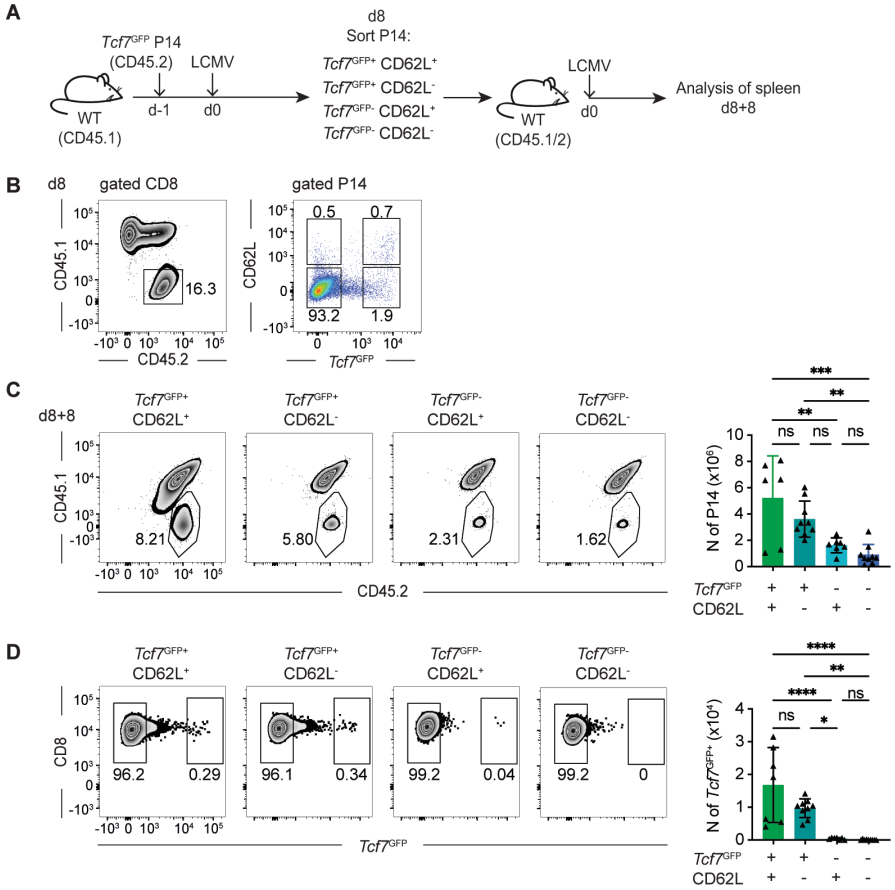

Fig. S4: Stemness of *Tcf7* and CD62L-defined CD8$^+$ T cell subsets

(**A**) B6 mice (CD45.1) were adoptively transferred with *Tcf7*^{GFP} P14 cells (CD45.2) and infected with LCMV Arm. At d8 p.i. the *Tcf7* and CD62L-defined P14 subsets were flow sorted and equal numbers of cells were transferred into secondary B6 recipients (CD45.1/2) that were then infected with LCMV Arm and analyzed 8 days later (d8+8). A second experiment was performed with LCMV WE. (**B**) Splenic P14 cells were analyzed for the expression of *Tcf7*^{GFP} versus CD62L at d8 p.i.. (**C**) Presence of secondary P14 cells deriving from the indicated d8 P14 subset (d8+8). (**D**) Presence of secondary *Tcf7*$^{GFP+}$ P14 cells deriving from the indicated d8 P14 subset (d8+8).

Data in (**C, D**) are compiled from 2 independent experiments with a total of n=6-8 mice per group. Data points in (**C, D**) represent individual mice. Bar graphs show means (±SD). Statistics are based on one-way ANOVA with Turkey's test with *: p<0.05; ***: p<0.001; ****: p <0.0001 and (ns) p>0.05.

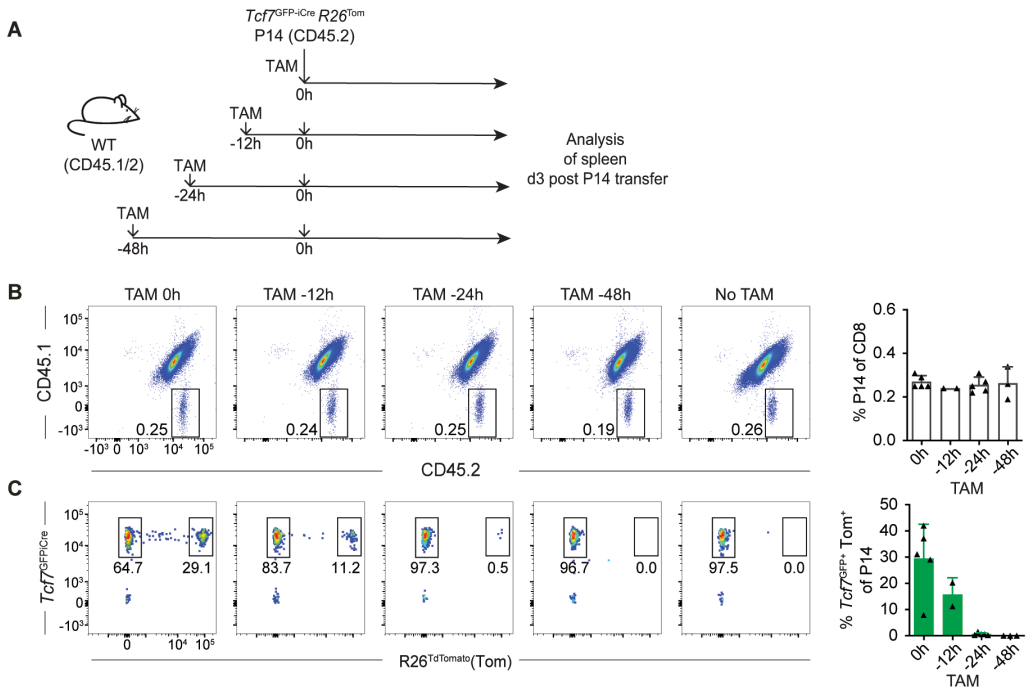

Fig. S5: Effective half-life of Tamoxifen (TAM)

(**A**) B6 recipients (CD45.1/2) were injected with a single dose of Tamoxifen (TAM) at 0h, 12h, 24h or 48h before the adoptive transfer of *Tcf7*$^{\text{GFP-iCre}}$ *R26*$^{\text{Tom}}$ P14 cells (CD45.2). (**B**) Three days after adoptive transfer, P14 cells were gated and (**C**) analyzed for the expression of Tom (*R26*$^{\text{Tom}}$). Data are compiled from 2 independent experiments with a total of n=2-5 mice per time point. Data points in (**B, C**) represent individual mice.

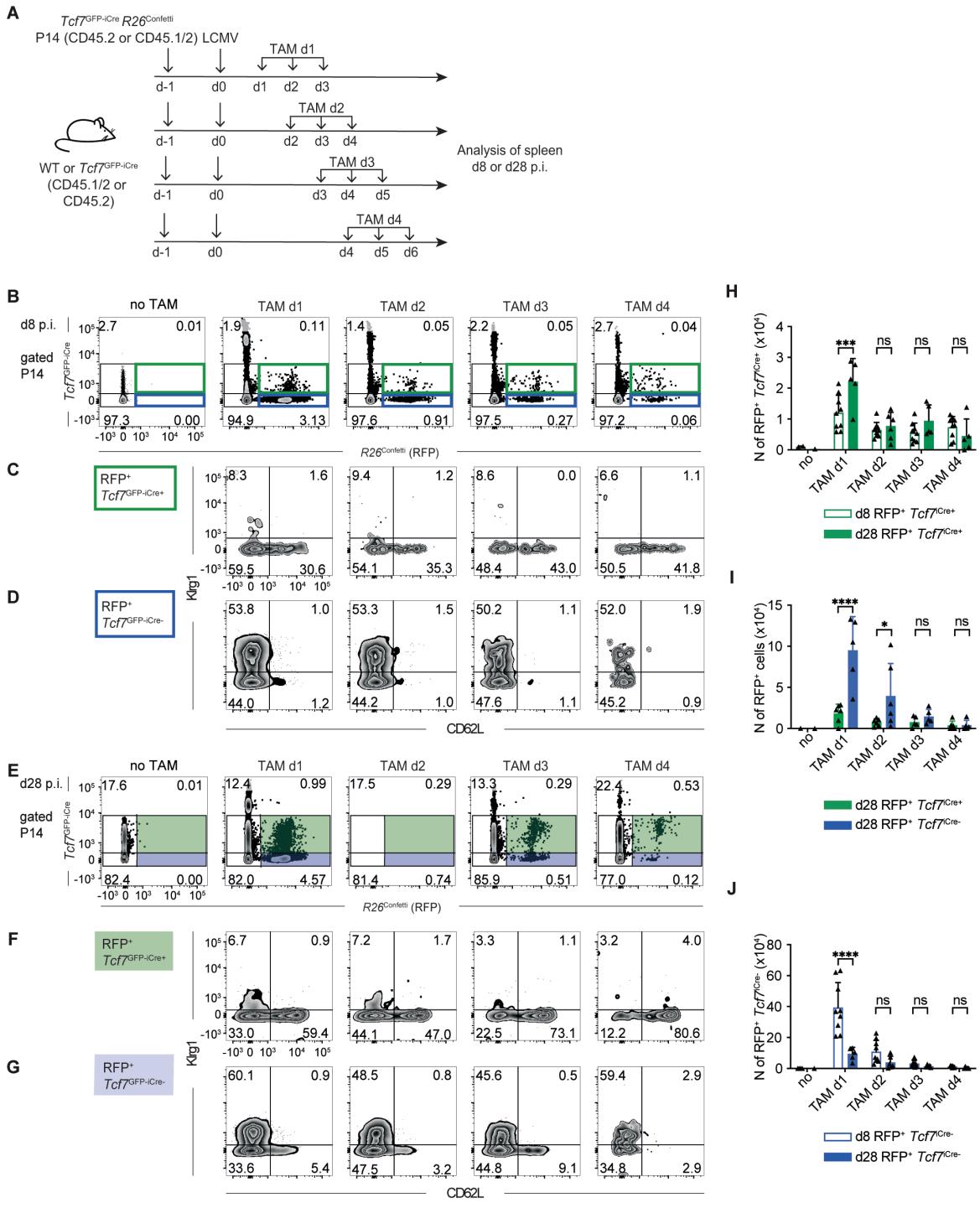

Fig. S6: Fate of *Tcf7*$^{+}$ CD8^{+} T cells present at d1, d2, d3 or d4 of infection

(**A**) B6 (CD45.2 or CD45.1/.2) or B6 *Tcf7*$^{\text{GFP-iCre}}$ mice (CD45.2) were adoptively transferred with *Tcf7*$^{\text{GFP-iCre}}$ *R26*$^{\text{Confetti}}$ P14 cells (CD45.2 or CD45.1/.2) and infected with LCMV WE one day later. Recipient mice were either left untreated (no) or injected with Tamoxifen (TAM) starting on d1

(TAM d1), d2, d3 or d4 p.i., daily for 3 consecutive days. Tamoxifen (TAM)-mediated induction of Cre recombinase activity in *Tcf7*$^{+}$ cells results in the stochastic and mutually exclusive expression of one of four fluorescent proteins (RFP, CFP, YFP or GFP), whereby only the analysis of the RFP-expressing population is shown. (**B**) Upon TAM injection, the *R26*$^{\text{Confetti}}$ allele yields P14 cells with very high GFP/YFP levels derived from the Confetti allele. These cells could be discriminated from cells expressing intermediate amounts of GFP derived from the *Tcf7*$^{\text{GFP-iCre+}}$ transgene. Hence, the GFP$^{\text{hi}}$ population of T cells was excluded from the analysis (see Methods for further explanation).

(**B, E**) Gated P14 cells present in the spleen were analyzed for the expression of RFP (*R26*$^{\text{Confetti}}$) versus intermediate levels of GFP (*Tcf7*$^{\text{GFP-iCre}}$). (**B**) d8 RFP^{+} *Tcf7*$^{\text{GFP-iCre+}}$ cells are highlighted (open green) and d8 RFP^{+} *Tcf7*$^{\text{GFP-iCre}}$ (open blue). (**E**) d28 RFP^{+} *Tcf7*$^{\text{GFP-iCre+}}$ cells are highlighted (filled green) and d28 RFP^{+} *Tcf7*$^{\text{GFP-iCre}}$ (filled blue). These subsets were analyzed for the expression of CD62L versus Klrg1 at d8 (**C, D**) and at d28 p.i. (**F, G**).

(**H-J**) The bar graphs show the numbers of (**H**) RFP^{+} *Tcf7*$^{\text{GFP-iCre+}}$ cells at d8 compared to d28 p.i. (**I**) RFP^{+} *Tcf7*$^{\text{GFP-iCre+}}$ versus RFP^{+} *Tcf7*$^{\text{GFP-iCre-}}$ cells at d28 p.i. and (**J**) RFP^{+} *Tcf7*$^{\text{GFP-iCre-}}$ cells at d8 compared to d28 p.i.

Data shown in (**H-J**) are compiled from 2-3 independent experiments with a total of n=6-9 mice per group. Data points in (**H-J**) represent individual mice. Bar graphs show means (±SD). Statistics in (**H-J**) is based on two-way ANOVA with Fisher LSD with ***: $p<0.001$; **: $p<0.01$; *: $p<0.05$; and ns (non-significant): $p>0.05$.

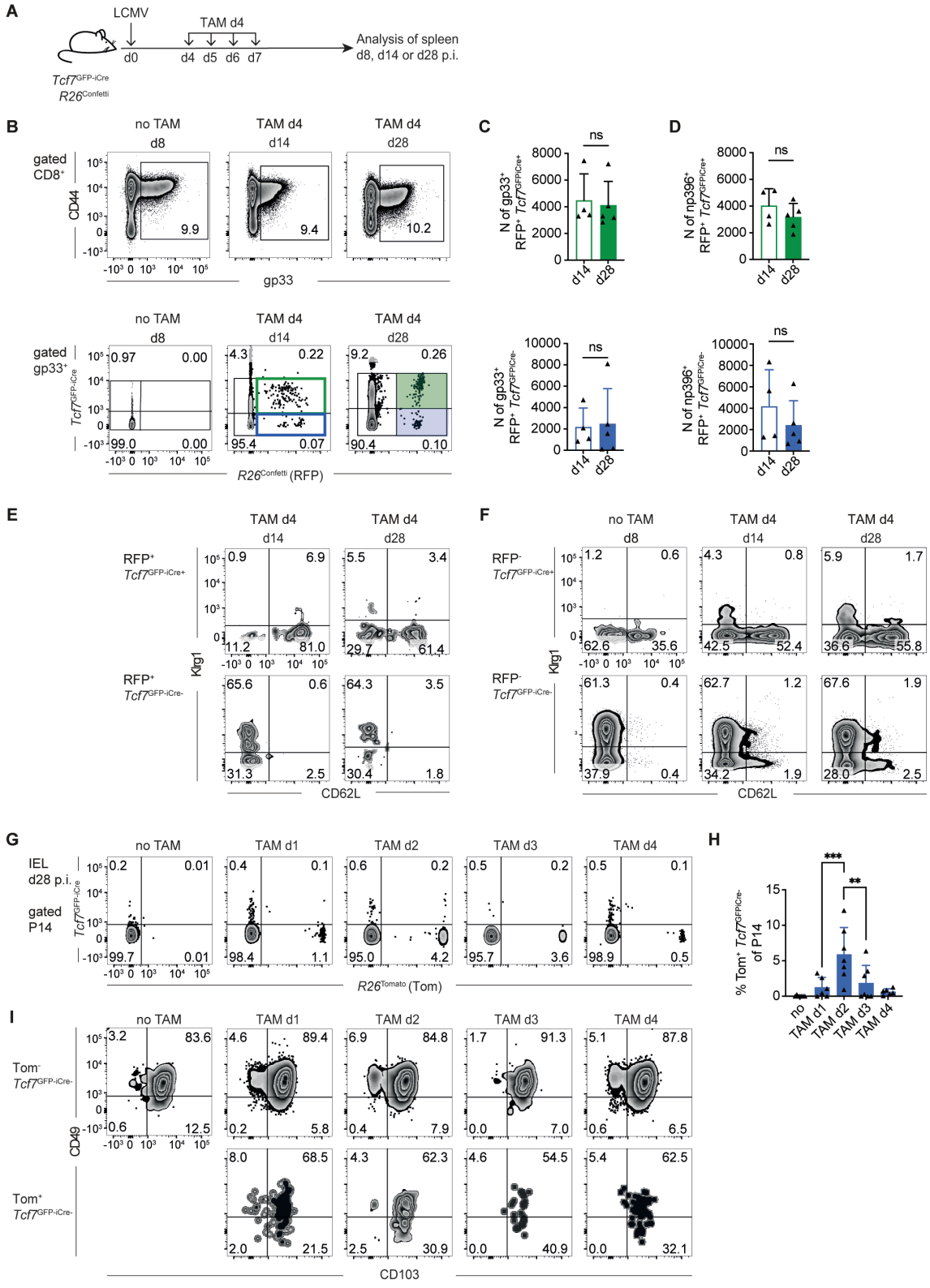
A
LCMV
TAM d4
d0
d4 d5 d6 d7
Analysis of spleen
d8, d14 or d28 p.i.
Tcf7GFP-iCre
R26Confetti
B
no TAM
TAM d4
TAM d4
d8
d14
d28
gated CD8+
CD44
gp33
gated gp33+
Tcf7GFP-iCre
R26Confetti (RFP)
C
N of gp33+ RFP+ Tcf7GFPiCre+
N of gp33+ RFP+ Tcf7GFPiCre-
ns
d14
d28
D
N of np396+ RFP+ Tcf7GFPiCre+
N of np396+ RFP+ Tcf7GFPiCre-
E
RFP+ Tcf7GFP-iCre+
RFP+ Tcf7GFP-iCre-
Klrg1
CD62L
F
no TAM
RFP- Tcf7GFP-iCre+
RFP- Tcf7GFP-iCre-
G
IEL d28 p.i.
gated P14
TAM d1
TAM d2
TAM d3
R26Tomato (Tom)
H
% Tom+ Tcf7GFPiCre- of P14
***
**
no TAM d1
TAM d2
TAM d3
TAM d4
I
Tom- Tcf7GFP-iCre-
Tom+ Tcf7GFP-iCre-
CD49
CD103

Fig. S7: Fate of polyclonal *Tcf7*$^{+}$ CD8^{+} T cells present at d4 of infection

(**A-F**) *Tcf7*$^{GFP\text{-}iCre}$ *R26*^{Confetti} mice were infected with LCMV WE and either left untreated (no) or injected with tamoxifen (TAM) starting on d4 p.i. daily for 4 consecutive days. (**B**) Presence of gp33 tetramer^{+} (gp33^{+}) CD44^{+} CD8^{+} T cells in untreated (no) or TAM treated mice analysed at d8, d14 or d28 p.i. (top). Gated gp33^{+} CD44^{+} CD8^{+} T cells were analyzed for the expression of R26^{Confetti} (RFP) versus *Tcf7*$^{GFP\text{-}iCre}$ (GFP). Numbers indicate the percentage of cells in the corresponding region i.e. excluding cells with high GFP levels. (**C**) Number of gp33^{+} CD44^{+} CD8^{+} T cells that are RFP^{+} *Tcf7*$^{GFP\text{-}iCre+}$ (top) or RFP^{+} *Tcf7*$^{GFP\text{-}iCre-}$ (bottom) at d14 compared to d28 p.i. (**D**) Number of np396^{+} CD44^{+} CD8^{+} T cells that are RFP^{+} *Tcf7*$^{GFP\text{-}iCre+}$ (top) or RFP^{+} *Tcf7*$^{GFP\text{-}iCre-}$ (bottom) at d14 compared to d28 p.i.

(**E**) Gated gp33^{+} RFP^{+} *Tcf7*$^{GFP\text{-}iCre+}$ (top) and RFP^{+} *Tcf7*$^{GFP\text{-}iCre-}$ cells (bottom) or (**F**) gp33^{+} RFP^{-} *Tcf7*$^{GFP\text{-}iCre+}$ and RFP^{+} *Tcf7*$^{GFP\text{-}iCre-}$ cells were analysed for the expression of CD62L versus Klrg1 on d14 and d28 p.i.

(**G-I**) *Tcf7*$^{GFP\text{-}iCre}$ *R26*^{Tom} P14 cells (CD45.2 or CD45.1/2) were adoptively transferred into B6 *Tcf7*$^{GFP\text{-}iCre}$ (CD45.2) or B6 recipients (CD45.2 or CD45.1/2) and infected with LCMV WE one day later. Recipient mice were either left untreated (no) or injected with a single dose of Tamoxifen (TAM) on d1 (TAM d1), d2, d3 or d4 p.i.. Gated P14 cells present among intestinal epithelial cells (IEL) were analyzed on d28 p.i. for (**G**) the expression of Tomato (*R26*^{Tomato}) versus GFP (*Tcf7*$^{GFP\text{-}iCre}$). (**H**) Percentage of Tom^{+} cells among P14 IEL. (**I**) Gated Tom^{+} and Tom^{-} *Tcf7*$^{GFP\text{-}iCre-}$ P14 IEL were analyzed for the expression of CD49d versus CD103.

Data in (**A-F**) are compiled from 2 independent experiments with a total of n=5 mice per group. Data in (**G-I**) are compiled from 3 independent experiments with a total of n=6-9 mice per group. Data points in (**C, D, H**) represent individual mice. Bar graphs show the mean (±SD). Statistics are based on non-paired two-tailed Student's test (**C, D**) One-Way ANOVA with LSD's test (**H**) whereby ****: p <0.0001; ***: p<0.001; **: p<0.01; *: p<0.05; and ns (non-significant): p>0.05.

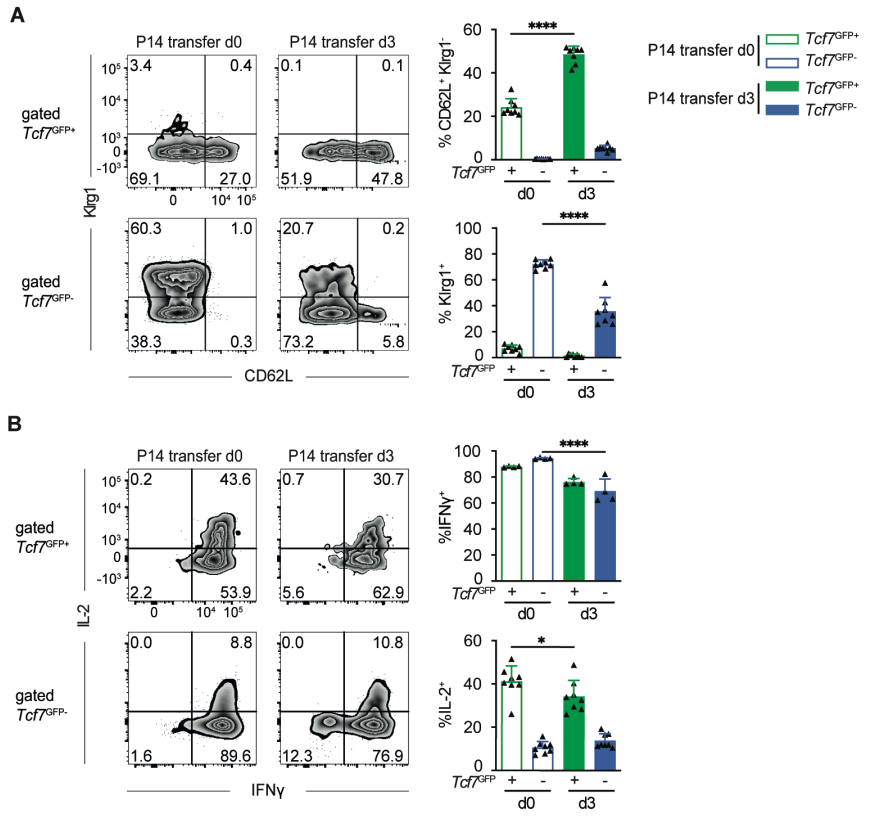

Fig. S8: Delayed recruitment of CD8$^+$ T cells into the response disfavors T_{TE} relative to T_{pCM} formation

(**A, B**) *Tcf7*^{GFP} P14 cells (10^4) (CD45.2) were transferred into B6 mice (CD45.1) and infected with LCMV Arm on the same day (P14 transfer d0). Alternatively, recipient mice were infected 3 days prior to the transfer of *Tcf7*^{GFP} P14 cells (P14 transfer d3). Gated *Tcf7*$^{GFP+}$ and *Tcf7*$^{GFP-}$ P14 cells were analyzed on d8 p.i. for the expression of (**A**) CD62L versus Klrg1 and (**B**) the production of IFNγ and IL-2 in response to *in vitro* restimulation with gp33 peptide. Data in (**A, B**) are compiled from 2 independent experiments with a total of n=8 mice per group. Data points in (**A, B**) represent individual mice. Bar graphs show the mean (±SD). Statistics is based on One-Way ANOVA with LSD's test (**A, B**) whereby ****: p <0.0001; ***: p<0.001; **: p<0.01; *: p<0.05; and ns (non-significant): p>0.05.

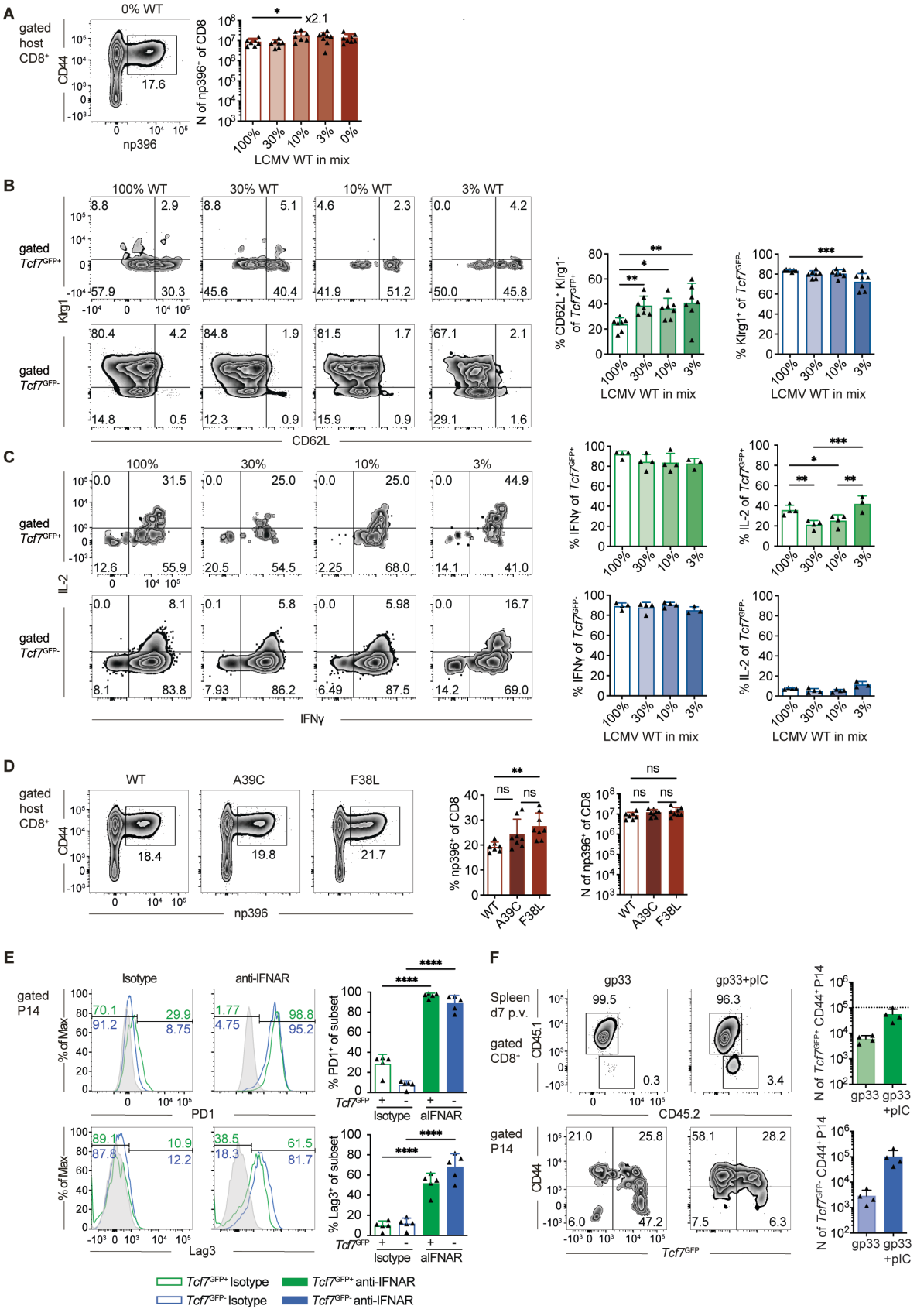
A
0% WT
gated host CD8+
CD44
17.6
np396
N of np396+ of CD8
x2.1
100% 30% 10% 3% 0%
LCMV WT in mix
B
100% WT
30% WT
10% WT
3% WT
gated Tcf7GFP+
gated Tcf7GFP-
Klrg1
CD62L
% CD62L+ Klrg1- of Tcf7GFP+
% Klrg1+ of Tcf7GFP-
LCMV WT in mix
C
100%
30%
10%
3%
gated Tcf7GFP+
gated Tcf7GFP-
IL-2
IFNγ
% IFNγ of Tcf7GFP+
% IL-2 of Tcf7GFP+
% IFNγ of Tcf7GFP-
% IL-2 of Tcf7GFP-
LCMV WT in mix
D
WT
A39C
F38L
gated host CD8+
CD44
18.4
19.8
21.7
np396
% np396+ of CD8
N of np396+ of CD8
ns
E
Isotype
anti-IFNAR
gated P14
% of Max
PD1
Lag3
% PD1+ of subset
% Lag3+ of subset
Tcf7GFP
Isotype
aIFNAR
Tcf7GFP+ Isotype
Tcf7GFP- Isotype
Tcf7GFP+ anti-IFNAR
Tcf7GFP- anti-IFNAR
F
gp33
gp33+pIC
Spleen d7 p.v.
gated CD8+
CD45.1
CD45.2
gated P14
CD44
Tcf7GFP
N of Tcf7GFP+ CD44+ P14
N of Tcf7GFP- CD44+ P14
gp33
gp33 +pIC

Fig. S9: Low antigen dose and affinity disfavors T_{TE} relative to T_{pCM} formation

(**A-C**) B6 mice (CD45.1/2) were adoptively transferred with naïve *Tcf7*^{GFP} P14 cells (CD45.2) before infection with a fixed but low dose of mixtures of different proportions of LCMV cl13 whose gp33 epitope is wild-type (WT) or has no measurable affinity for the P14 TCR (F38L) (Δgp33). (**A**) Recipient mice were analysed on d8 p.i. for the presence of host-derived np396 tetramer^{+} CD8^{+} T cells. (**B, C**) *Tcf7*$^{GFP+}$ and *Tcf7*$^{GFP-}$ P14 cells were analyzed for (**B**) the expression of CD62L versus Klrg1 and (**C**) the production of IFNγ and IL-2 in response to *in vitro* restimulation with gp33 peptide.

(**D**) B6 mice (CD45.1/2) were adoptively transferred with naïve *Tcf7*^{GFP} P14 cells (CD45.2) and infected with a low dose of LCMV cl13 whose gp33 epitope has normal (wild-type (WT)), reduced (A39C) or no affinity (F38L, Δgp33) for the P14 TCR. Recipient mice were analysed on d8 p.i. for the presence of host-derived np396 tetramer^{+} CD8^{+} T cells.

(**E**) B6 mice (CD45.1) were adoptively transferred with naïve *Tcf7*^{GFP} P14 cells (CD45.2) and infected with LCMV Arm one day later (d0). Recipient mice were treated with anti-NK1.1 (to deplete NK cells) and anti-IFNAR or isotype control Ab at d-1. Gated *Tcf7*$^{GFP+}$ and *Tcf7*$^{GFP-}$ cells were analysed for PD-1 (top) and LAG-3 expression (bottom) at d8 p.i.

(**F**) B6 mice (CD45.1/2) were adoptively transferred with naïve *Tcf7*^{GFP} P14 cells (CD45.2) (10^6) before vaccination with gp33 peptide or gp33 peptide plus poly(I:C) (pIC). P14 cells were analyzed 7 days post-vaccination (p.v.) for the expression of CD44 versus *Tcf7*^{GFP}. The abundance of CD44^{+} *Tcf7*$^{GFP+}$ P14 cells in the spleen is compared to the input of naïve P14 cells (assuming an initial take of 10%), indicated by the broken line.

The data in (**A, B, D**) are compiled from 2 independent experiments with a total of n=7-8 mice per group. The data in (**C, E, F**) are from a single experiment with n= 4-5 mice per group. Data points in (**A-F**) represent individual mice. Means (±SD) are shown. Statistics in (**A-E**) are based One-Way ANOVA with Fisher's LSD test whereby ****: p <0.0001; ***: p<0.001; **: p<0.01; *: p<0.05; and ns (non-significant): p>0.05.

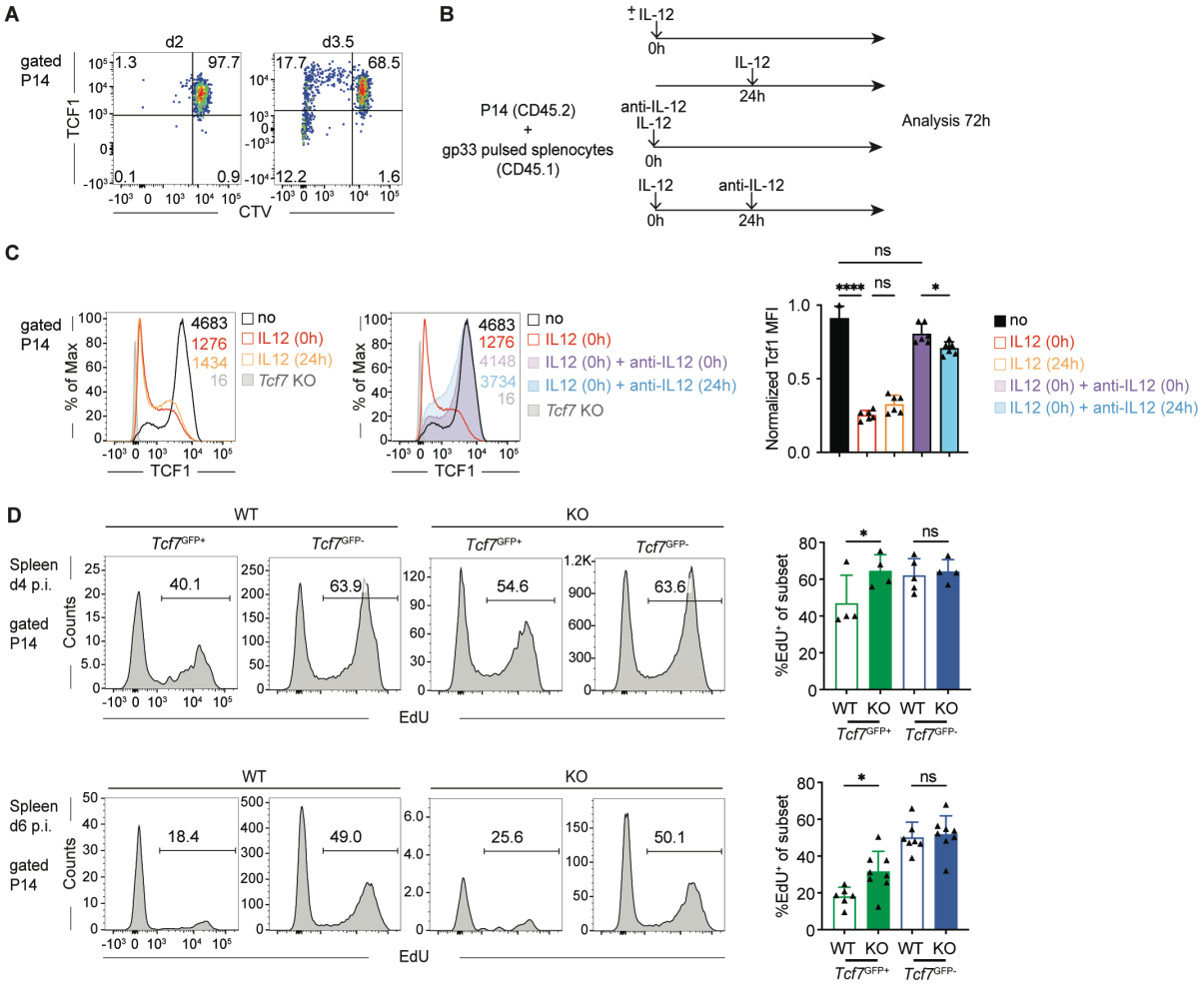

Fig. S10: Role of inflammatory signals in TCF1 downregulation and of TCF1 in cell cycling.

(A) B6 mice (CD45.1/2) were adoptively transferred with CTV-labelled naïve P14 cells (CD45.2) (10^6) before infection with LCMV WE. Gated P14 cells were analyzed for CTV versus TCF1 expression on d2 and d3.5 p.i.

(B, C) Purified P14 cells (CD45.2) from naïve mice were stimulated *in vitro* with gp33 peptide-pulsed splenocytes (CD45.1). IL-12 was added at the start of the culture (0h) and anti-IL-12 was added 24h later (before the first cell division) to restrict the action of IL12 to the first 24h of culture. Alternatively, IL-12 was added after 24h (before the first cell division) (**B**). (**C**) Gated P14 cells were analysed for TCF1 expression after 72h of culture.

(D) WT *Tcf7*^{GFP} P14 cells or *Tcf7*$^{-/-}$ (KO) *Tcf7*^{GFP} P14 cells (CD45.2) were transferred into B6(CD45.1) recipients one day prior to infection with LCMV Arm and analysed on d4 or d6 p.i..

Two hours prior to sacrifice mice were injected with Edu. Gated *Tcf7*$^{GFP+}$ and *Tcf7*$^{GFP-}$ P14 cells were analysed for EdU incorporation.

Data in (**A**) are representative of 4 independent experiments, data in (**C**) derive from 3-6 independent determinations in a single experiment and data in (**D**) are pooled from 2 independent experiments with a total of n=4-8 mice per time point and group. Data points in (**C, D**) represent individual mice. Means (±SD) are shown. Statistics in (**C, D**) is based on One-Way ANOVA with Turkey's test (**C**) or with LSD's Fisher (**D**) whereby ****: p <0.0001; ***: p<0.001; **: p<0.01; *: p<0.05; and ns (non-significant): p>0.05.

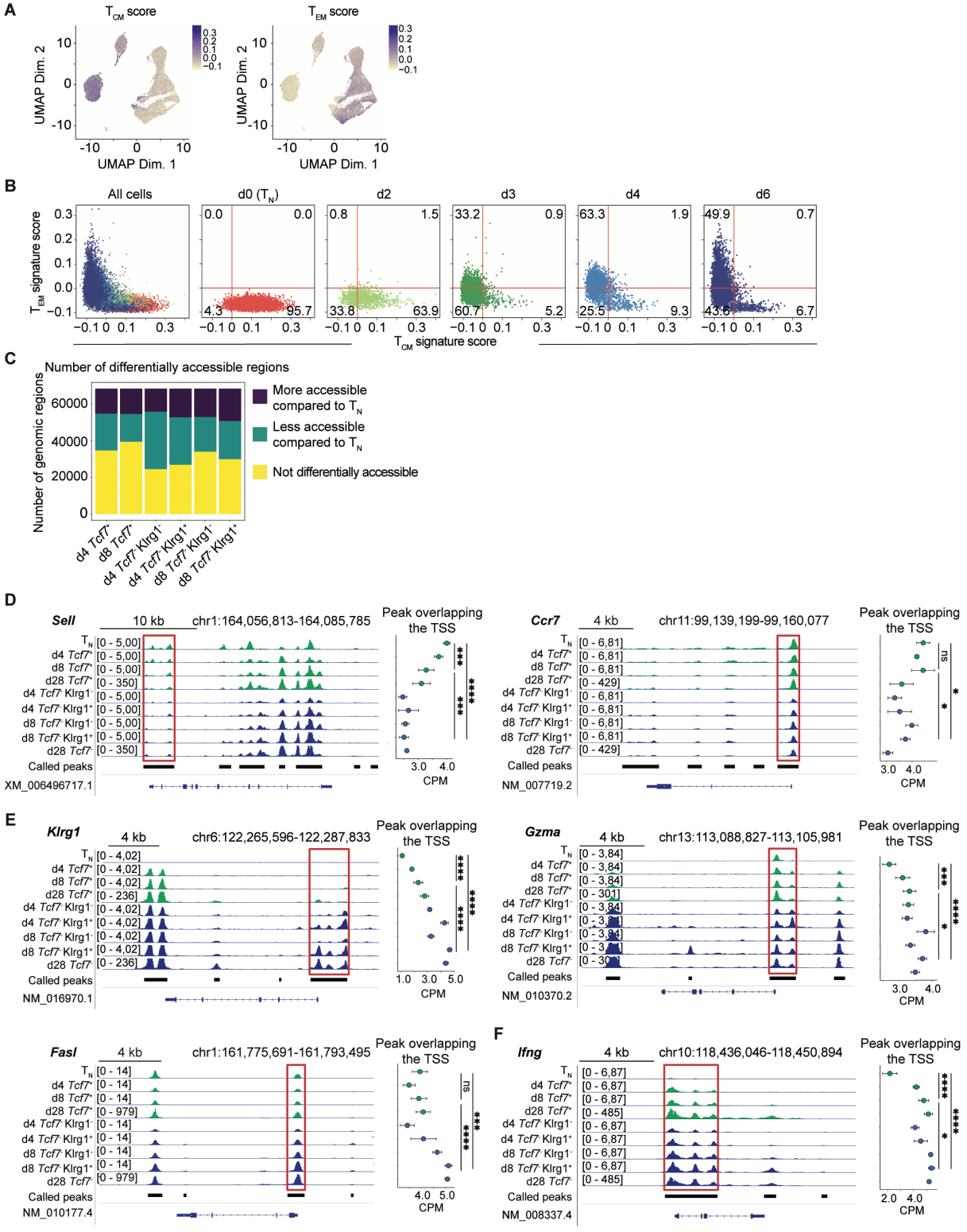
A
T_CM score
T_EM score
UMAP Dim. 2
UMAP Dim. 1
B
All cells
d0 (T_N)
d2
d3
d4
d6
T_EM signature score
T_CM signature score
C
Number of differentially accessible regions
Number of genomic regions
More accessible compared to T_N
Less accessible compared to T_N
Not differentially accessible
d4 Tcf7+
d8 Tcf7+
d4 Tcf7- Klrg1-
d4 Tcf7- Klrg1+
d8 Tcf7- Klrg1-
d8 Tcf7- Klrg1+
D
Sell
10 kb
chr1:164,056,813-164,085,785
Peak overlapping the TSS
Ccr7
4 kb
chr11:99,139,199-99,160,077
Called peaks
XM_006496717.1
NM_007719.2
CPM
E
Klrg1
chr6:122,265,596-122,287,833
Gzma
chr13:113,088,827-113,105,981
NM_016970.1
NM_010370.2
Fasl
chr1:161,775,691-161,793,495
NM_010177.4
F
Ifng
chr10:118,436,046-118,450,894
NM_008337.4

Fig. S11: Stable loss of the T_{pCM} gene signature occurs upon *Tcf7* downregulation and precedes stable acquisition of a T_{TE} gene signature

(**A, B**) B6 mice (CD45.1) were adoptively transferred with naïve *Tcf7*^{GFP} P14 cells (CD45.2) and infected with LCMV Arm. P14 cells (CD45.2) cells were flow sorted on d0 (naïve, T_N), d2, d3, d4 and d6 post-infection (p.i.) and subjected to scRNAseq. (**A**) UMAP plot of individual P14 cells colored according to their expression level of genes differentially expressed between d30 *Tcf7*$^{GFP+}$ cells (upregulated genes = T_{CM} signature score) versus d30 *Tcf7*$^{GFP-}$ cells (downregulated genes = T_{EM} signature score) (*22*). (**B**) Individual P14 cells were analyzed for the overall intensity of the T_{CM} versus the T_{EM} signature score.

(**C**) B6 mice (CD45.1) were adoptively transferred with naïve *Tcf7*^{GFP} P14 cells (CD45.2) and infected with LCMV Arm. *Tcf7*$^{GFP+}$, *Tcf7*$^{GFP-}$ Klrg1^{-} and *Tcf7*$^{GFP-}$ Klrg1^{+} P14 cells (CD45.2) were flow sorted on d4 or d8 p.i. and, together with naïve P14 cells (T_N), subjected to ATACseq analysis. The bar graph depicts global accessibility change in the indicated population compared to T_N cells, whereby the number of less accessible (dark blue), more accessible (green) and equally accessible (yellow) genomic regions is indicated.

(**D-F**) Genome browser view of sequencing read coverage (dark blue tracks) at **(D)** the *Sell* (CD62L) *and Ccr7* loci, (**E**) the *Klrg1, GzmA, FasL* loci and (**F**) the *Ifng* locus. Black horizontal lines depict accessible regions based on peak calling. The dot graph depicts means (±SD) of the normalized accessibility at the called peak overlapping the transcriptional start site (TSS) of the indicated genes in the different populations (n=3 samples).

Dot plots in (**D-F**) show means (±SD) and statistics is based on One-Way ANOVA with Fisher's LSD test with ****: p <0.0001; ***: p<0.001; **: p<0.01; *: p<0.05; and ns (non-significant): p>0.05.

SUPPLEMENTARY TABLE LEGENDS

Data file S1. Number of cells captured for single-cell RNA sequencing

The table depicts numbers of cells for each sample (d0 to d6) prior to quality control (left column) and numbers of cells retained for further analysis after quality control.

Data file S2. Gene signatures defining T_{pCM}, T_{CM}, T_{EM} and T_{TE} cells.

Sheet 1: Genes differentially expressed (abs(log2FC)>1.5 & adj. p-value<0.05) between d8 *Tcf7*$^+$ (T_{pCM}) versus d8 *Tcf7*$^-$ P14 cells (*22*).

Sheet 2: Genes differentially expressed (abs(log2FC)>1.5 & adj. p-value<0.05) between d30 *Tcf7*$^+$ (T_{CM}) versus d30 *Tcf7*$^-$ P14 cells (T_{EM}) (*22*).

Sheet 3: Genes differentially expressed (abs(log2FC)>1.5 & adj. p-value<0.05) between d7 Klrg1$^+$ (T_{TE}) versus d7 Klrg1$^-$ P14 cells (*47*).

Data file S3. Correlation between the up-regulation of T_{pCM} or T_{TE} signature genes and chromatin accessibility changes

Sheet 1: List of genes up-regulated in d8 *Tcf7*$^+$ (T_{pCM}) cells (see **Data file S2**) that were more accessible in the indicated population of cells.

Sheet 2: List of genes up-regulated in d7 Klrg1$^+$ (T_{TE}) cells (see **Data file S2**) that were more accessible in the indicated population of cells.